Calculations of electron scattering from cadmium

Michael J. Berrington,* Christopher J. Bostock,† Dmitry V. Fursa, and Igor Bray
ARC Centre for Antimatter-Matter Studies, Curtin University, G.P.O. Box U1987, Perth, WA 6845, Australia

R. P. McEachran
Centre for Antimatter-Matter Studies, Research School of Physical Sciences and Engineering, Australian National University, Canberra, ACT 0200, Australia

A. D. Stauffer
Department of Physics and Astronomy, York University, Toronto, Ontario, Canada, M3J 1P3
(Received 22 December 2011; published 9 April 2012)

Electron scattering from the ground state of cadmium atoms has been investigated theoretically using the convergent close-coupling, relativistic convergent close-coupling, relativistic optical potential, and relativistic distorted-wave methods. Elastic and inelastic differential cross sections, Stokes parameters, and spin-asymmetry parameters have been calculated and compared with available experimental and theoretical results. We find, in general, very good agreement between the theories and experiment.

DOI: 10.1103/PhysRevA.85.042708 PACS number(s): 34.80.Bm, 34.80.Dp, 34.80.Nz, 34.80.Pa

I. INTRODUCTION

Accurate theories describing electron scattering from heavy-metal atoms play a vital role in modeling plasmas found in the lighting industry and fusion research. Furthermore, understanding the role of spin in electron-atom interactions is a key component to progress in exciting research areas such as spintronics [1,2] and quantum information [3].

Cadmium ($Z = 48$) is a sufficiently heavy target for spin-orbit (relativistic) effects to manifest in low-energy electron-scattering measurements. There are several experimental studies for electron-cadmium scattering in the literature. The most comprehensive study is that of Marinkovic *et al.* [4], who measured relative differential cross sections (DCSs) for elastic scattering and excitation of the $(5s5p)\,^3P_1^o$, $(5s5p)\,^3P_2^o$, $(5s5p)\,^1P_1^o$, $(5s6s)\,^3S_1$, $(5s6s)\,^1S_0$, $(5s5d)\,^1D_2$, $(5s6p)\,^1P_1^o$, $(5s7s)\,^1S_0$, $[(5s6d)\,^1D_2 + (5s7p)\,^1P_1^o]$, $(5s8s)\,^1S_0$, and $[(5s7d)\,^1D_2 + (5s8p)\,^1P_1^o]$ levels. Measurements were taken for several energies ranging between 3.4 and 85 eV. Nogueira *et al.* [5] have reported absolute DCSs for elastic scattering in the 60–150 eV energy range. These data were put on an absolute scale by measuring relative DCSs for excitation of the $(5s5p)\,^1P_1^o$ state. Relative DCSs were also measured by Sullivan *et al.* [6] in the energy range 3–5 eV at a high-energy resolution at scattering angles of 24°, 54°, 90°, and 120°. Electron-impact coherence parameters (EICPs) for the $(5s5p)\,^1P_1^o$ state were measured by Piwinski *et al.* [7]. Data were collected for incident electron energies of 60, 80, and 100 eV at scattering angles in the 5°–50° range. Bartsch *et al.* [8] measured the spin-asymmetry parameter S_A for elastic scattering. The S_A parameter is equivalent to the Sherman function [9] for elastic scattering. Measurements were taken at various energies between 0.3 and 9.0 eV. In addition, S_A was measured at a high-energy resolution between 0.3 and 7 eV at a scattering angle of 110°.

There have been limited theoretical investigations of electron-cadmium scattering. Madison *et al.* [10] carried out semirelativistic distorted-wave (DW) calculations for elastic scattering and excitation of the $(5s5p)\,^3P_1^o$, $(5s5p)\,^3P_2^o$, $(5s5p)\,^1P_1^o$, $(5s6s)\,^1S_0$, $(5s5d)\,^1D_2$, and $(5s6p)\,^1P_1^o$ states. Srivastava *et al.* [11,12] applied a fully relativistic distorted-wave (RDW) method to the excitation of the P and D states, producing cross sections and EICPs. McEachran and Stauffer [13] calculated the asymmetry parameter S_A for elastic scattering using a RDW method with a nonrelativistic polarization potential calculated via the polarized-orbital method. Szmytkowski and Sienkiewicz [14] performed similar calculations with a relativistic polarization potential.

Recently the relativistic convergent close-coupling (RCCC) method has been used to resolve a long-standing discrepancy between theory and experiment for the spin-asymmetry parameter (Sherman function) in elastic e-Cd scattering [15]. Here we present further details of the calculation, together with a range of results for elastic and inelastic differential cross sections, integrated cross sections, Stokes parameters, and electron-impact coherence parameters. Results of the nonrelativistic convergent close-coupling (CCC) method, and also the relativistic optical potential (ROP) and RDW methods, are presented for comparison. Agreement between the theories and experiment is generally very good for most observables of interest, except in the case of the calculation of the Sherman function. The nonrelativistic CCC method gives identically zero for the Sherman function, and the ROP results differ significantly from experiment. The success of the RCCC method is due to first an *ab initio* treatment of relativistic spin-orbit effects, and second the fact that the theory is unitary. This will be discussed further in Sec. III.

The paper is organized as follows: Section II contains a brief overview of the CCC, RCCC, ROP and RDW methods with details applicable to electron scattering from cadmium. In Sec. III we present results of our calculations for angle differential cross sections across a range of incident electron energies for elastic scattering and excitation of low-energy

*Deceased.
†c.bostock@curtin.edu.au

states. Stokes parameters (P_1, P_2, P_3) and EICPs (P_L, γ, P_+) are presented for the excitation of the $(5s5p)\,^1P_1$ state. The spin-asymmetry parameter S_A is presented for low-energy elastic scattering. Atomic units are used throughout the paper.

II. CALCULATION METHODS

A. RCCC method

The recently developed RCCC method has been applied to the calculation of electron scattering from quasi-one-electron targets [16–19] and quasi-two-electron targets [20,21]. Comprehensive details of the RCCC method for both quasi-one- and quasi-two-electron targets have recently been given [22]. In the case of e-Cd scattering, the cadmium atom is modeled as two active valence electrons above an inert $[\mathrm{Kr}]4d^{10}$ Dirac-Fock core. The $[\mathrm{Kr}]4d^{10}$ Dirac-Fock core orbitals are obtained using the GRASP package [23]. For the valence electrons, a set of one-electron orbitals is obtained by diagonalization of the Cd^+ quasi-one-electron Dirac-Coulomb Hamiltonian in a relativistic (Sturmian) L-spinor basis [24]. The set of orbitals obtained contains $5s$–$23s$, $5p_j$–$23p_j$, $5d_j$–$22d_j$, and $5f_j$–$21f_j$ ($j = l \pm 1/2$) orbitals. Two-electron configuration interaction calculations are then performed to obtain wave functions for the Cd atom. The choice of two-electron configurations was such that one electron is in $5s_{1/2}$,$6s_{1/2}$; $5p_{1/2}$,$6p_{1/2}$; $5p_{3/2}$, $6p_{3/2}$; or $5d_{3/2}$, $5d_{5/2}$ orbitals while the other electron occupies any of the one-electron orbitals allowed by selection rules. We have found that this model provides a sufficiently accurate description of Cd wave functions.

We have also added phenomenological one- and two-electron polarization potentials to improve the accuracy of the calculated Cd wave functions [25,26]. The phenomenological one-electron V^{pol} and two-electron V^{diel} core polarization potentials allow us to take into account more accurately the effect of closed inert shells on the active electron. The falloff radii r_c^{pol} and r_c^{diel} of these potentials are chosen to obtain the best representation of target state energies and optical oscillator strengths (OOSs), while the static dipole polarizability of the inert core α_c is taken from accurate calculations [27,28]. In the case of Cd we chose $\alpha_c = 4.971a_0^3$, $r_c^{\mathrm{diel}} = 1.7$, and an l-dependent r_c^{pol} with values 1.7, 1.3, 2.0, and 1.9 for $l = 0$, 1, 2, and 3, respectively. The energy levels of the first 10 states used in the calculation are listed in Table I together with experimental levels listed by NIST [29]. The OOSs for the $(5s5p)\,^3P_1$ and $(5s5p)\,^1P_1$ states are listed in Table II. We find that reduction of the falloff parameter r_c^{diel} below the value of 1.7 does not lead to further substantial reduction of the OOS for the resonance $(5s^2)\,^1S_0$–$(5s5p)\,^1P_1$ transition. Our OOS value of 1.39 is larger than the most recent recommended value of 1.2 [30]; however, it proved to be in good agreement with the older value of 1.4 obtained by Lurio and Novick [31]. According to the measurements of Goebel and Hohm [32] the experimental static dipole polarizability of Cd is $49.65a_0^3$. With our target model we obtain a value of $38.25a_0^3$. This is substantially lower than the experimental measurement and is an indication of the imperfection in the $[\mathrm{Kr}]4d^{10}$ inert core model because a large part of the static dipole polarizability comes from inner core excitations. In the present work we have chosen the polarization potential parameters to obtain the most accurate energy levels and oscillator strengths within the present structure model; this is at the expense of obtaining an accurate value for the static dipole polarizability.

TABLE I. Energy levels of the Cd states of interest calculated by diagonalizing the target in the RCCC and CCC methods. Experimental levels listed by NIST [29] are also shown.

				Energy (eV)		
Configuration	Term	J	Parity	CCC	RCCC	Expt.[a]
$5s^2$	$^1S_0$	0.0	1	0.000	0.000	0.000
$5s5p$	$^3P^o_0$	0.0	−1	4.068	3.748	3.734
$5s5p$	$^3P^o_1$	1.0	−1	4.125	3.826	3.800
$5s5p$	$^3P^o_2$	2.0	−1	4.250	4.003	3.946
$5s5p$	$^1P^o_1$	1.0	−1	5.426	5.243	5.417
$5s6s$	$^3S_1$	1.0	1	6.364	6.375	6.383
$5s6s$	$^1S_0$	0.0	1	6.643	6.650	6.610
$5s5d$	$^1D_2$	2.0	1	7.419	7.394	7.342
$5s6p$	$^1P^o_1$	1.0	−1	7.450	7.390	7.427
$5s7s$	$^1S_0$	0.0	1	7.842	7.843	7.822
$5s6d$	$^1D_2$	2.0	1	8.131	8.103	8.076
$5s7p$	$^1P^o_1$	1.0	−1	8.167	8.112	8.120
$5s8s$	$^1S_0$	0.0	1	8.468	8.321	8.295
$5s7d$	$^1D_2$	2.0	1	8.685	8.451	8.411
$5s8p$	$^1P^o_1$	1.0	−1	8.810	8.479	8.438
Ionization limit				8.989	8.996	8.993

[a]Reference [29].

For the scattering calculations we chose two models: a 55-state calculation that includes only the bound states, and a 200-state calculation that includes both bound and continuum states.

The generated target states are then used to expand the total wave function of the electron-cadmium scattering system and to formulate a set of relativistic Lippmann-Schwinger equations for the T-matrix elements. In this latter step, the relativistic Lippmann-Schwinger equations for the T-matrix elements have the following partial wave form:

$$T_{fi}^{\Pi J}(k_f\kappa_f,k_i\kappa_i) = V_{fi}^{\Pi J}(k_f\kappa_f,k_i\kappa_i) + \sum_n \sum_\kappa \int\!\!\!\!\!\!\diagup dk \times \frac{V_{fn}^{\Pi J}(k_f\kappa_f,k\kappa)T_{ni}^{\Pi J}(k\kappa,k_i\kappa_i)}{E-\epsilon_n^N-\epsilon_{k'}+i0}. \quad (1)$$

The notation in Eq. (1), the matrix elements, and the method of solution using a hybrid OpenMP-MPI parallelization suitable for high-performance supercomputing architectures is given in Ref. [22]. The T-matrix elements obtained from the solution of Eq. (1) are used to determine the scattering amplitudes, which in turn are used to calculate the differential cross sections and other observables of interest.

TABLE II. Oscillator strengths of the Cd ground state.

Transition	RCCC	CCC	RDW	Expt.
$(5s^2)\,^1S_0$–$(5s5p)\,^3P_1$	0.0045	0.0032	0.0066	0.0019[a]
$(5s^2)\,^1S_0$–$(5s5p)\,^1P_1$	1.39	1.42	2.26	1.42,[b] 1.2[c]

[a]References [30,31].
[b]Reference [31].
[c]Reference [30].

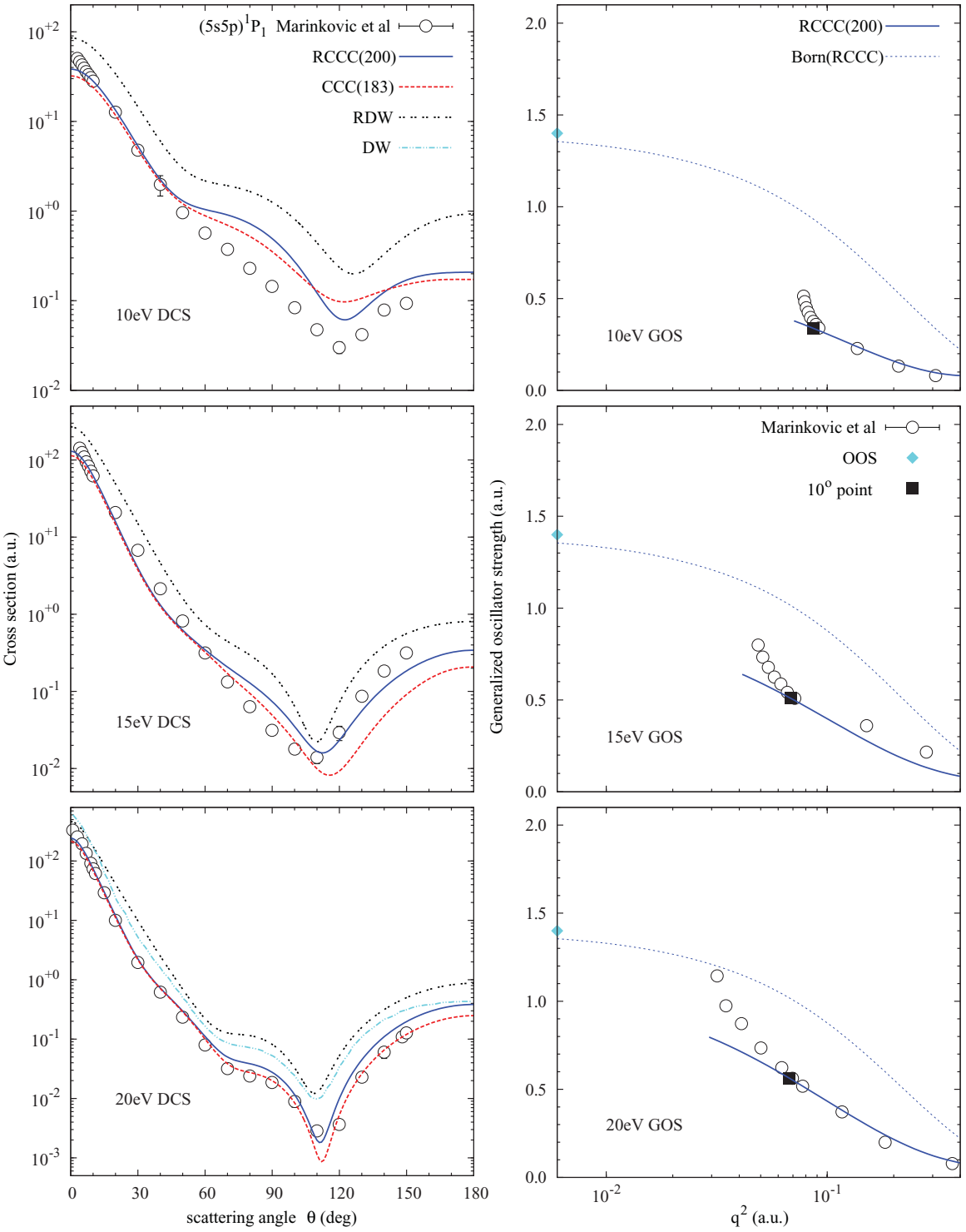

FIG. 1. (Color online) DCS and GOS for the excitation of the $(5s5p)\,^1P_1$ state of cadmium at incident electron energies of 10, 15, and 20 eV. The CCC(183), RCCC(200), and RDW calculations are described in the text. The DW results are due to Madison *et al.* [10]. The experimental results for the GOS have been calculated from the experimental DCS of Marinkovic *et al.* [4].

B. CCC method

The application of the nonrelativistic CCC formalism to electron scattering from quasi-two-electron atoms has been described by Fursa and Bray [25]. Both RCCC and CCC calculations share the same model of the Cd atom, two active valence electrons above an inert [Kr]$4d^{10}$ core. Core orbitals are obtained from a Hartree-Fock calculation for the ground state of the Cd^+ ion. One-electron orbitals for the valence electron are obtained by diagonalizing the Cd^+ Hamiltonian in a Laguerre basis. These calculations are carried out for each $l \leqslant 3$. The parameters of the Laguerre basis (exponential cutoffs and number of functions) were chosen to be similar

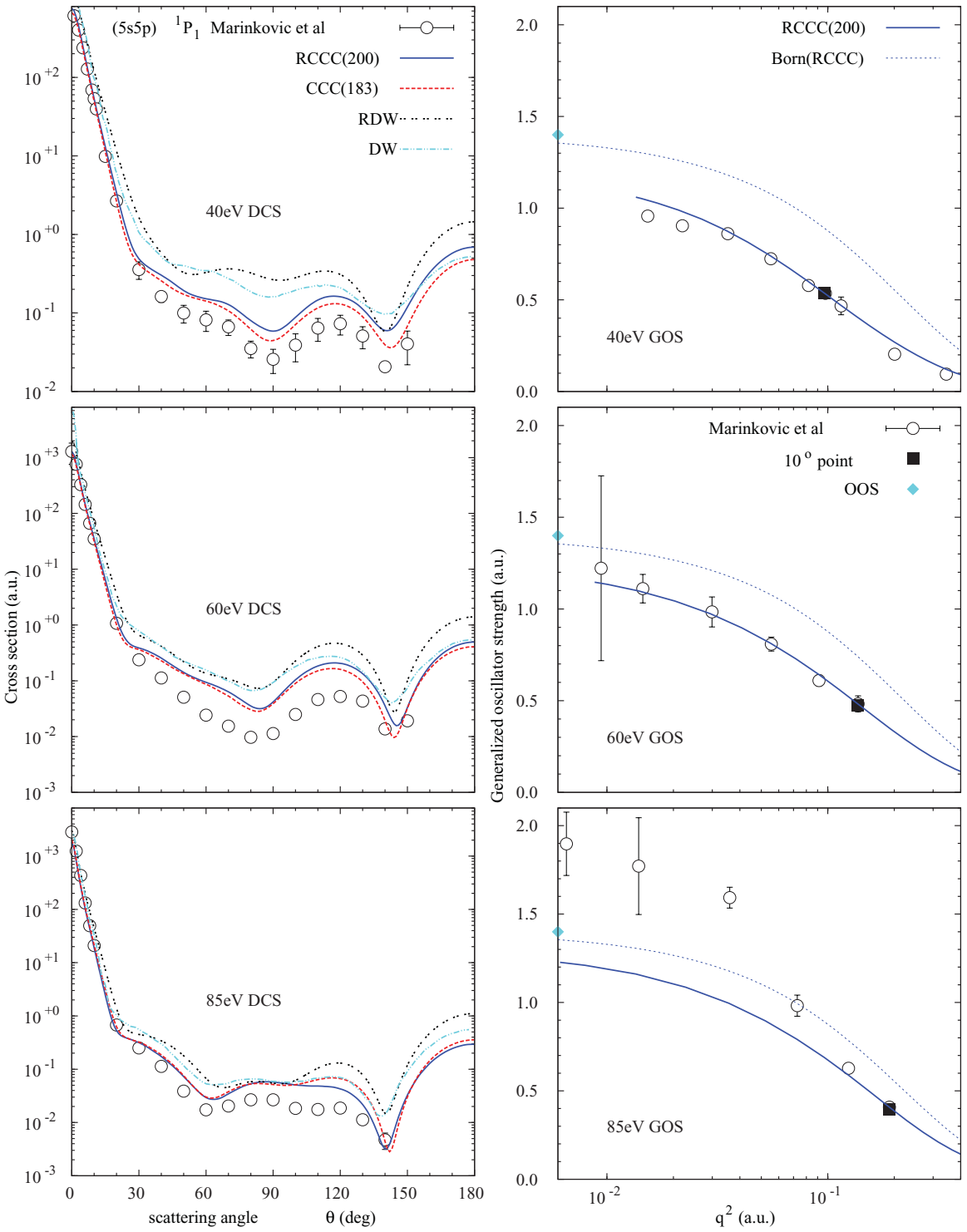

FIG. 2. (Color online) Same as in Fig. 1 but at incident electron energies of 40, 60, and 85 eV.

to the L-spinor basis discussed in the previous section for the RCCC method. A phenomenological one-electron polarization potential [25] is added to the Cd^+ Hamiltonian to model core excitation processes. The parameters of this polarization potential are chosen to fit the ground-state energy of Cd^+ to experimental values.

The resulting set of one-electron orbitals is used in a standard two-electron configuration-interaction calculation [33] to obtain a set of cadmium-atom wave functions. The choice of two-electron configurations was made in a similar manner as we have done for the RCCC calculation, namely one electron is in a $5s$, $6s$, $5p$, $6p$, and $5d$ orbital while the other electron is in any other orbital that is allowed by selection rules. To further model core polarization effects, a two-electron polarization potential [25] is added to the cadmium Hamiltonian. The parameters of this

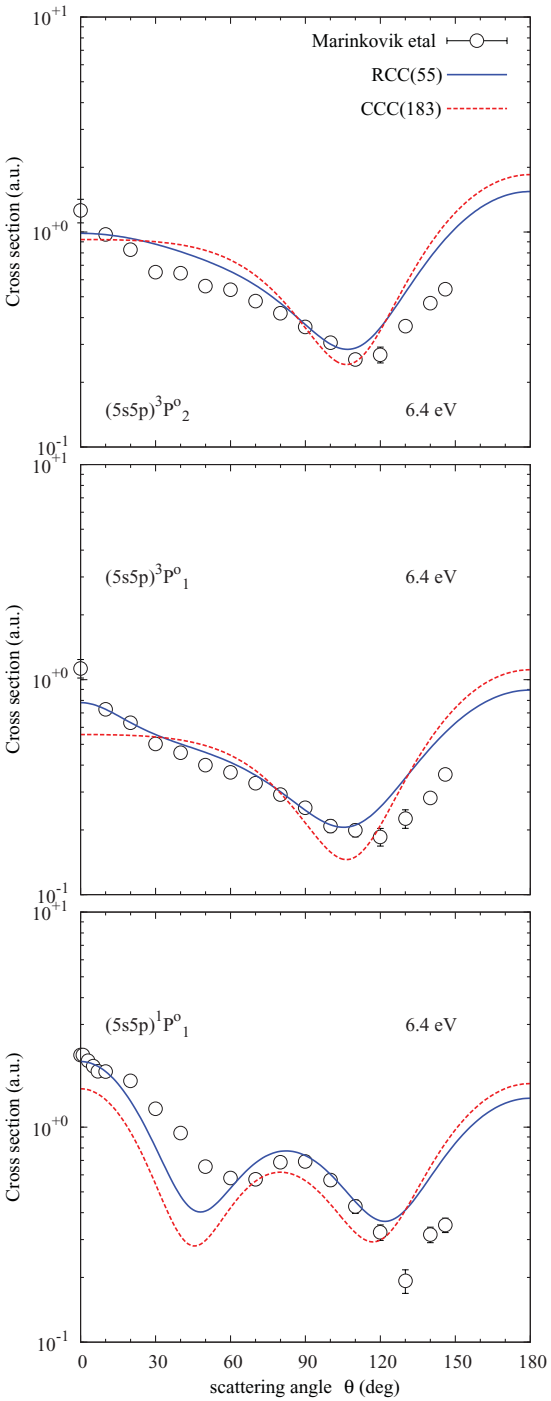

FIG. 3. (Color online) DCS for the excitation of various states of cadmium at an incident electron energy of 6.4 eV. Theory and experiment as in Fig. 1.

potential are selected to fit the ground-state energy and optical oscillator strength as closely as possible to experimental values.

Energy levels calculated in the CCC structure model are presented in Table I. The oscillator strength for the resonance $(5s5p)\,^1P_1$–$(5s^2)\,^1S_0$ transition was fitted to an experimental value of 1.42 [31,34]. The cadmium-atom ground-state static dipole polarizability was calculated to be $37.3a_0^3$, with the $(5s5p)\,^1P^o$–$(5s5s)\,^1S$ transition being the major contributor. Similar to the RCCC model this result is significantly below the experimentally determined value of $49.65a_0^3$ [32]; the reasons for this discrepancy are the same as for the RCCC method.

The total number of states generated in the CCC structure calculations is 183 with 33 bound states and the rest are positive-energy pseudostates. Close-coupling calculations have been performed in two models, the 33-state model and a 183-state model. The difference between these two models gives an indication of the importance of the coupling to ionization channels.

The major relativistic effect in e-Cd scattering calculations is due to singlet-triplet mixing of the target wave functions. The account of this has been done as described in Ref. [35]. Briefly, the nonrelativistic CCC calculations provide a set of scattering amplitudes $f^S_{\pi_f,s_f,l_f,m_f;\pi_i,s_i,l_i,m_i}(\boldsymbol{k}_f)$ where the total spin is S, the final (initial) target state parity is π_f (π_i), the spin is s_f (s_i), the orbital angular momentum is l_f (l_i), its projection on the Z axis of the collision frame is m_f (m_i), and $\boldsymbol{k}_f$ is the momentum of the scattered electron. We transform these scattering amplitudes to the amplitudes describing transitions between fine-structure levels J_f and J_i,

$$f^{\mu_f,\mu_i}_{\pi_f,J_f,M_f;\pi_i,J_i,M_i}(\gamma_f,\gamma_i;\boldsymbol{k}_f) = \sum_{S,m_f,\sigma_f,m_i,\sigma_i} C^{J_fM_f}_{l_fm_f,s_f\sigma_f} C^{SM_S}_{\frac{1}{2}\mu_f,s_f\sigma_f} C^{J_iM_i}_{l_im_i,s_i\sigma_i} \times C^{SM_S}_{\frac{1}{2}\mu_i,s_i\sigma_i} f^S_{\pi_f,s_f,l_f,m_f;\pi_i,s_i,l_i,m_i}(\boldsymbol{k}_f), \quad (2)$$

where μ_f (μ_i) are final (initial) projectile spin projections on the Z axis of the collision frame and the index γ distinguishes states with the same orbital angular momentum, spin, and parity. The amplitudes in the intermediate coupling scheme are then formed as

$$F^{\mu_f,\mu_i}_{\pi_f,J_f,M_f;\pi_i,J_i,M_i}(\beta_f,\beta_i;\boldsymbol{k}_f) = \sum_{\gamma_f,\gamma_i} C^{\beta_f}_{\gamma_f}\, C^{\beta_i}_{\gamma_i}\, f^{\mu_f,\mu_i}_{\pi_f,J_f,M_f;\pi_i,J_i,M_i}(\gamma_f,\gamma_i;\boldsymbol{k}_f), \quad (3)$$

where the index β distinguishes target states with the same total angular momentum J and parity π. Coefficients C^{γ}_{β} are obtained by diagonalizing the Breit-Pauli Hamiltonian (with only the one-body spin-orbit term) in the basis of the Cd target states obtained from the nonrelativistic structure calculations. We note that such a semirelativistic treatment does not take into account any relativistic effects for the incident electron.

Finally, we note that semirelativistic DW calculations of Madison *et al.* [10] have a similar approach in the description of the Cd target wave functions; however, the projectile electron wave function is treated in a fully relativistic way using the Schrödinger form of the Dirac equation [36].

C. The ROP and RDW methods

The elastic cross sections and the Sherman function were calculated using the ROP method while all the inelastic cross sections and Stokes parameters were determined from the RDW method. As both of these methods have recently been

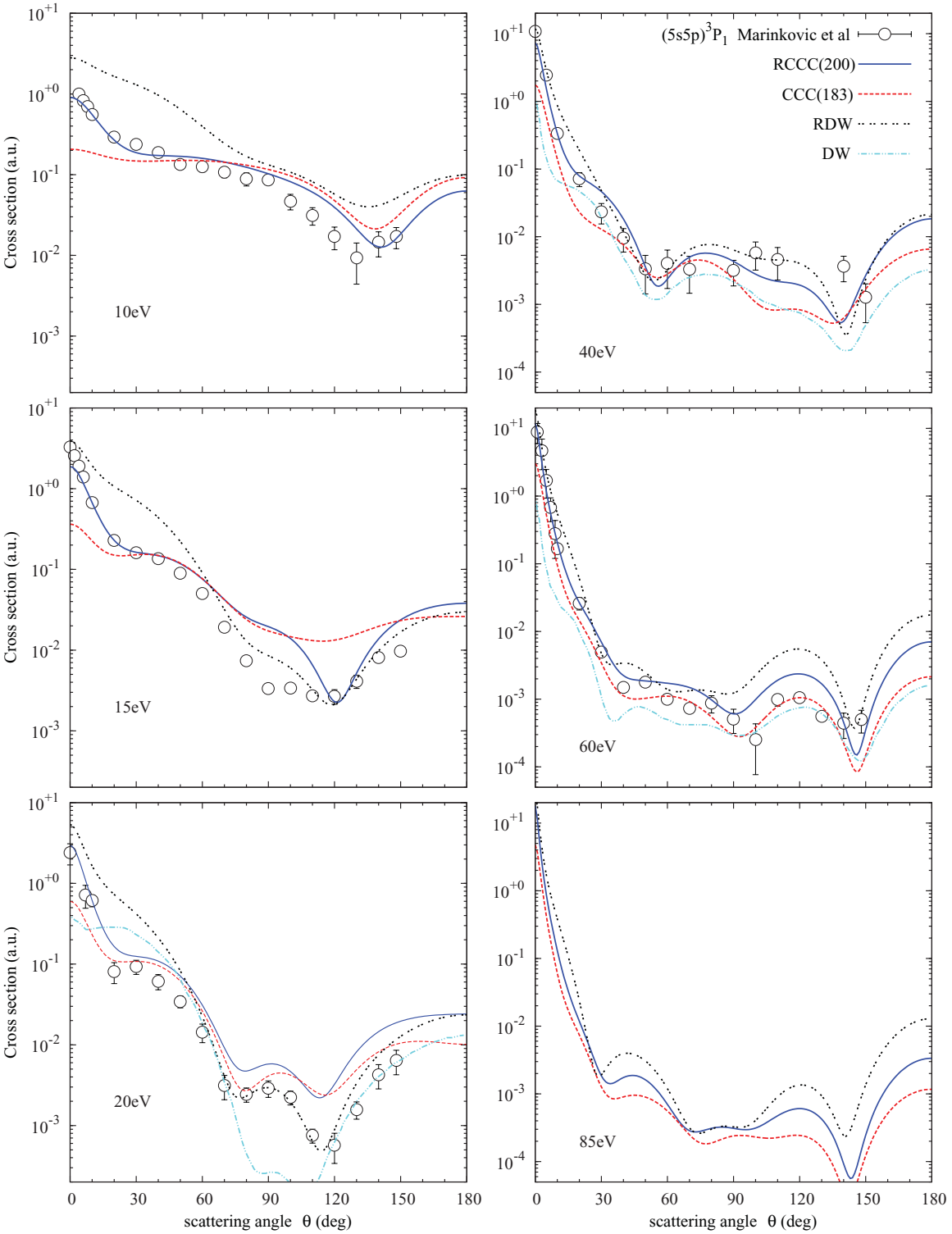

FIG. 4. (Color online) DCS for the excitation of the $(5s5p)\,^3P_1$ state of cadmium at incident electron energies of 10, 15, 20, 40, 60, and 85 eV. Theory and experiment as in Fig. 1.

described in some detail in the literature [37,38], only a brief discussion with respect to their application to cadmium is given here.

The atomic wave functions for cadmium were produced in a frozen-core manner using a modified version of the multiconfiguration Dirac-Fock code of Grant *et al.* [39]. The wave functions of Cd^{2+} were first determined in a fully varied manner. Next, together with the dipole polarization potential of Cd^{2+}, a frozen-core calculation of the ground $5s$ state of Cd^+ was performed. Here the polarization potential was scaled by a factor of 1.0705 in order to reproduce the experimental ionization energy of Cd^+. Finally, the ground-state wave

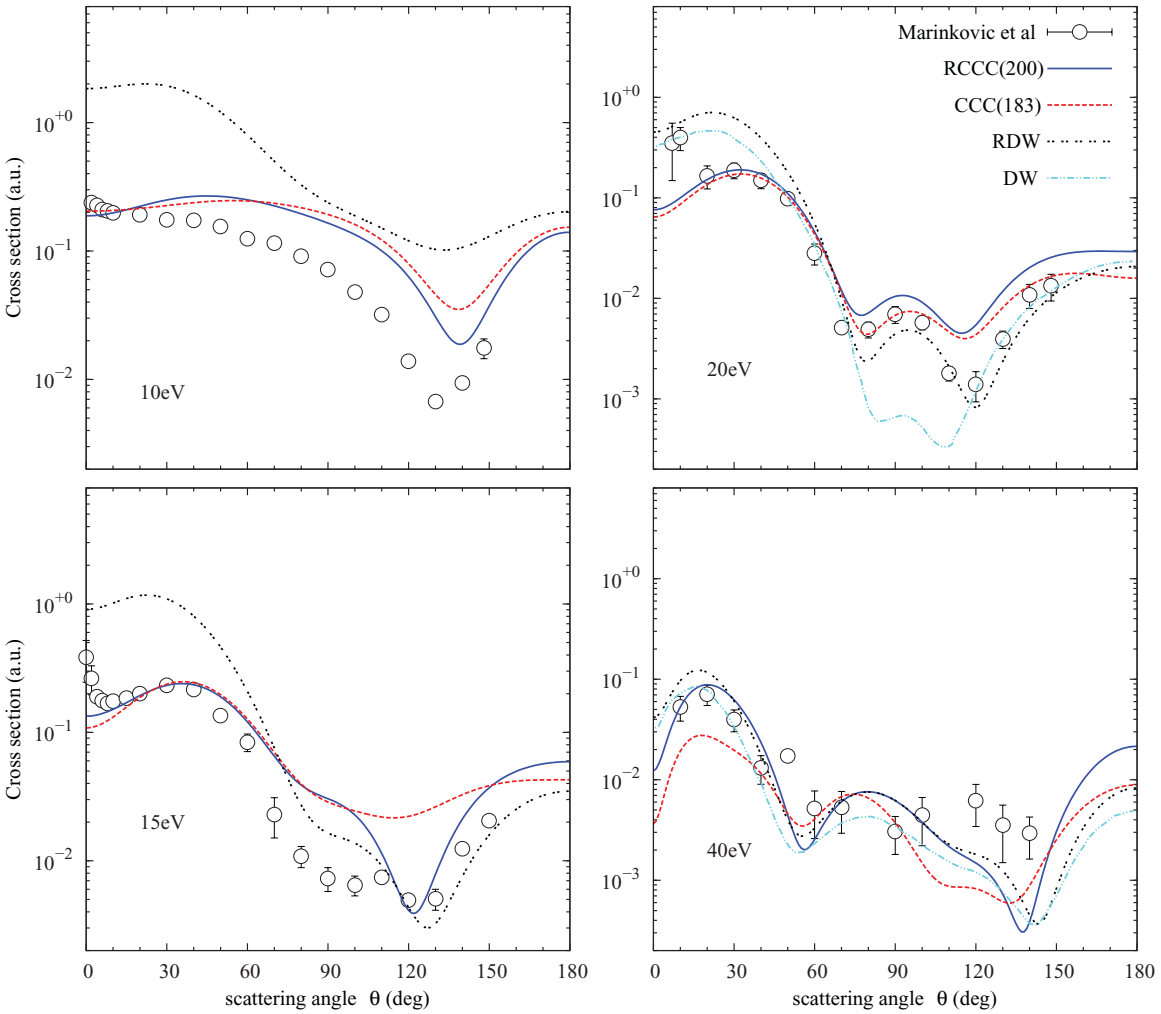

FIG. 5. (Color online) DCS for the excitation of the $(5s5p)\,^3P_2$ state of cadmium at incident electron energies of 10, 15, 20, and 40 eV. Theory and experiment as in Fig. 1.

function of Cd was determined in the fixed field of the Cd^{2+} ion plus its polarization potential while the excited states of Cd were determined in the fixed field of the Cd^+ ion. The same wave functions were used in both the ROP and RDW methods.

In the case of elastic scattering using the ROP method, the static potential as well as the dipole polarization potential of Cd were included in the calculation. This latter potential was scaled to yield the experimental value of $49.65a_0^3$ for the dipole polarizability. Furthermore, whenever inelastic channels (excitation and ionization) were open, the above potentials were augmented by an imaginary and nonlocal optical potential in order to simulate absorption effects. In particular, the following discrete states were included to simulate excitation, namely $6s\,^1S_0$, $5p\,^1P_1$, $5p\,^3P_1$, $5d\,^1D_2$, $5d\,^3D_2$, $6p\,^1P_1$, and $6p\,^3P_1$, while the following continuum states simulated ionization: $\epsilon s\,^1S_0$, $\epsilon p\,^1P_1$, $\epsilon p\,^3P_1$, $\epsilon d\,^1D_2$, $\epsilon d\,^3D_2$, $\epsilon f\,^1F_3$, and $\epsilon f\,^3F_3$. Here ϵ represents the energy of the ionized electron.

In the RDW method for inelastic scattering, a transition from an initial channel specified by the quantum numbers $i\mu_i$ to a final channel specified by the quantum numbers $f\mu_f$ is described in terms of the T-matrix element:

$$T(M,\mu_i,\mu_f;\hat{\boldsymbol{k}}_f) = \langle \phi_f(JM)\, F^-_{k_f\mu_f}(\boldsymbol{r},\sigma)|V-U| \times \mathcal{A}[\phi_i(00)\, F^+_{k_i\mu_i}(\boldsymbol{r},\sigma)]\rangle. \quad (4)$$

Here the quantum numbers μ_i and μ_f specify the spin projections of the incident and outgoing electrons, respectively, while the quantum number i denotes the ground state of the atom and f denotes an excited state of the atom. The corresponding wave functions of these states are given by $\phi_i(00)$ and $\phi_f(JM)$ while $F^+_{k_i\mu_i}(\boldsymbol{r},\sigma)$ and $F^-_{k_f\mu_f}(\boldsymbol{r},\sigma)$ denote the distorted waves in the initial and final channels, respectively. Furthermore, J and M are the total angular momentum quantum numbers of the final state while $\hat{\boldsymbol{k}}_f$ specifies the direction of the outgoing electron. The potential V in Eq. (4) is the interaction potential between the incident electron and the atom while U is the so-called distortion potential and $\mathcal{A}$ is the usual antisymmetrization operator. In the this work, the potential U was chosen to be the static potential of the ground state in the initial channel i while U was taken to be the spherically averaged static potential of the excited state in the final channel f as well as in Eq. (4).

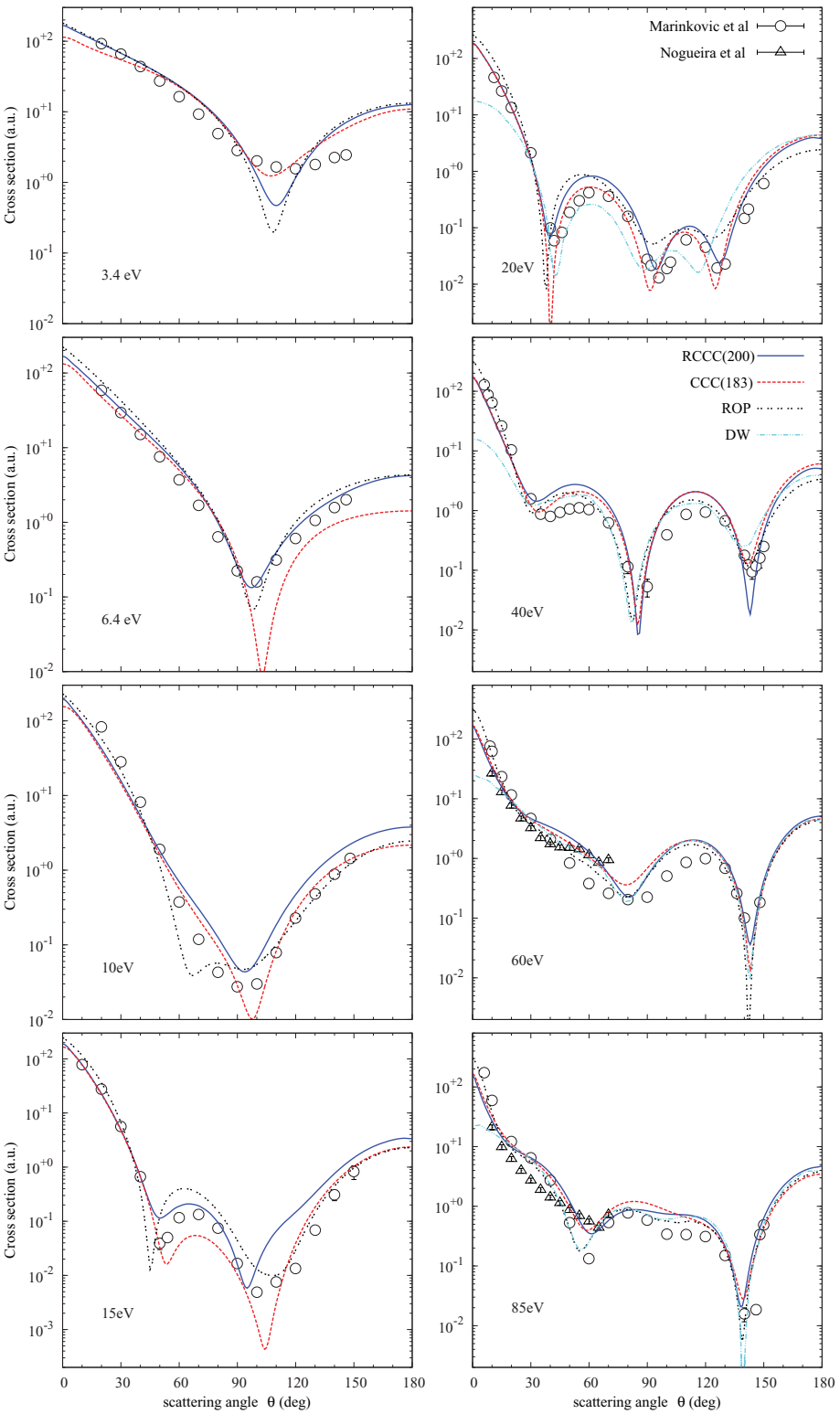

FIG. 6. (Color online) DCS for the elastic scattering from the ground state of cadmium at incident electron energies of 3.4, 6.4, 10, 15, 20, 40, 60, and 85 eV. Present RCCC, CCC, and ROP methods are described in the text. DW results are due to Madison *et al.* [10]. Experimental results are due to Marinkovic *et al.* [4] and Nogueira *et al.* [5].

The corresponding scattering amplitudes which describe all these excitation processes are defined in terms of the T-matrix elements as

$$f(M,\mu_i,\mu_f;\hat{\boldsymbol{k}}_f) = (2\pi)^2 \left(\frac{k_f}{k_i}\right)^{\frac{1}{2}} T(M,\mu_i,\mu_f;\hat{\boldsymbol{k}}_f). \quad (5)$$

If the incident beam of electrons is unpolarized and there is no spin analysis of the corresponding outgoing particles, then we can define the differential cross section for excitation as

$$\sigma(\hat{\boldsymbol{k}}_f) = \frac{1}{2} \sum_{M\mu_i\mu_f} |f(M,\mu_i,\mu_f;\hat{\boldsymbol{k}}_f)|^2. \quad (6)$$

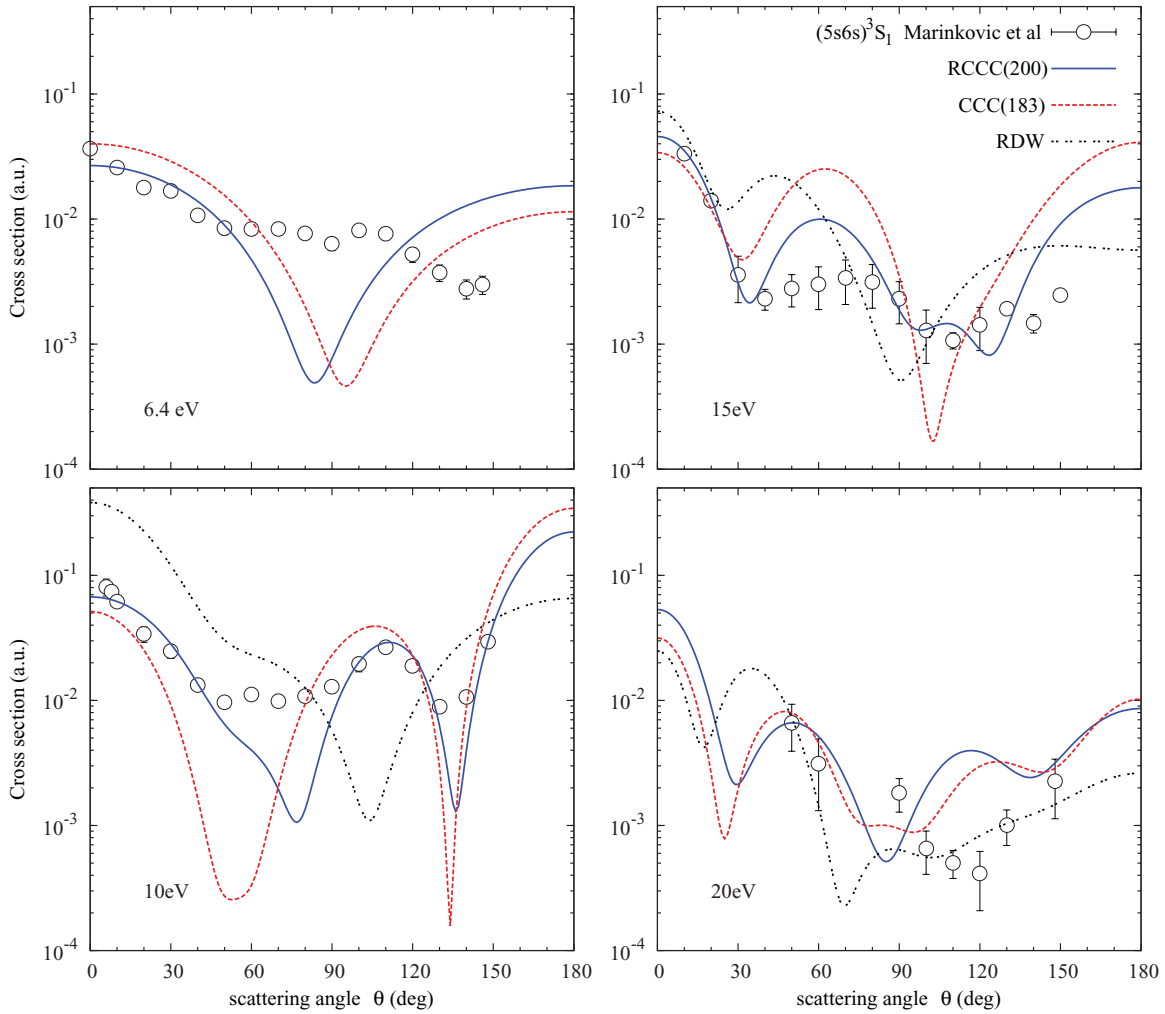

FIG. 7. (Color online) DCS for the excitation of the $(5s6s)\,^3S_1$ state of cadmium at incident electron energies of 6.4, 10, 15, and 20 eV. Theory and experiment as in Fig. 1.

III. RESULTS

We compare in this section results of our calculations with experimental DCSs measured by Nogueira *et al.* [5] for elastic scattering and by Marinkovic *et al.* [4] for elastic scattering and a large number of excitations. In both works no absolute measurements were performed. In the former work the ratio of the elastic DCS to the resonance $(5s5p)\,^1P_1$ transition was measured and put on absolute scale by normalizing the $(5s5p)\,^1P_1$ generalized oscillator strength (GOS) to the corresponding optical oscillator strength. In the latter work no absolute normalization of the cross sections was attempted; however, cross sections were normalized with respect to the resonance transition at 90°. Due to the importance of the resonance transition normalization we start this section with detailed discussion of $(5s5p)\,^1P_1$ DCS and GOS.

A. Differential cross sections

GOS may be calculated from the DCS measurements of Marinkovic *et al.* [4] using the expression

$$f = \tfrac{1}{2}(E_i - E_f)(k_i/k_f)q^2(d\sigma/d\Omega), \tag{7}$$

where E_i and E_f are the initial and final electron energies, respectively; k_i and k_f are the initial and final electron wave numbers, respectively; $d\sigma/d\Omega$ is the measured DCS; and q^2 is given by

$$q^2 = k_i^2 + k_f^2 - 2k_i k_f \cos\theta, \tag{8}$$

with

$$E_i + k_i^2/2 = E_f + k_f^2/2. \tag{9}$$

In Figs. 1 and 2 DCSs and GOSs for the excitation of the $(5s5p)\,^1P_1$ state of cadmium are presented. Present 183-state CCC and the 200-state RCCC results are presented together with present RDW results, and DW calculations of Madison *et al.* [10] and experimental results of Marinkovic *et al.* [4]. The experimental GOS values were calculated using Eqs. (7)–(9) with the experimentally determined excitation energy ($\Delta e = E_i - E_f$). The experimental relative GOSs of Marinkovic *et al.* [4] were put on an absolute scale by normalizing to the RCCC GOS values at an angle of 10°. The DCS values were modified by the same factor. The value of q^2 corresponding to the 10° angle is denoted by a square on each GOS curve. The

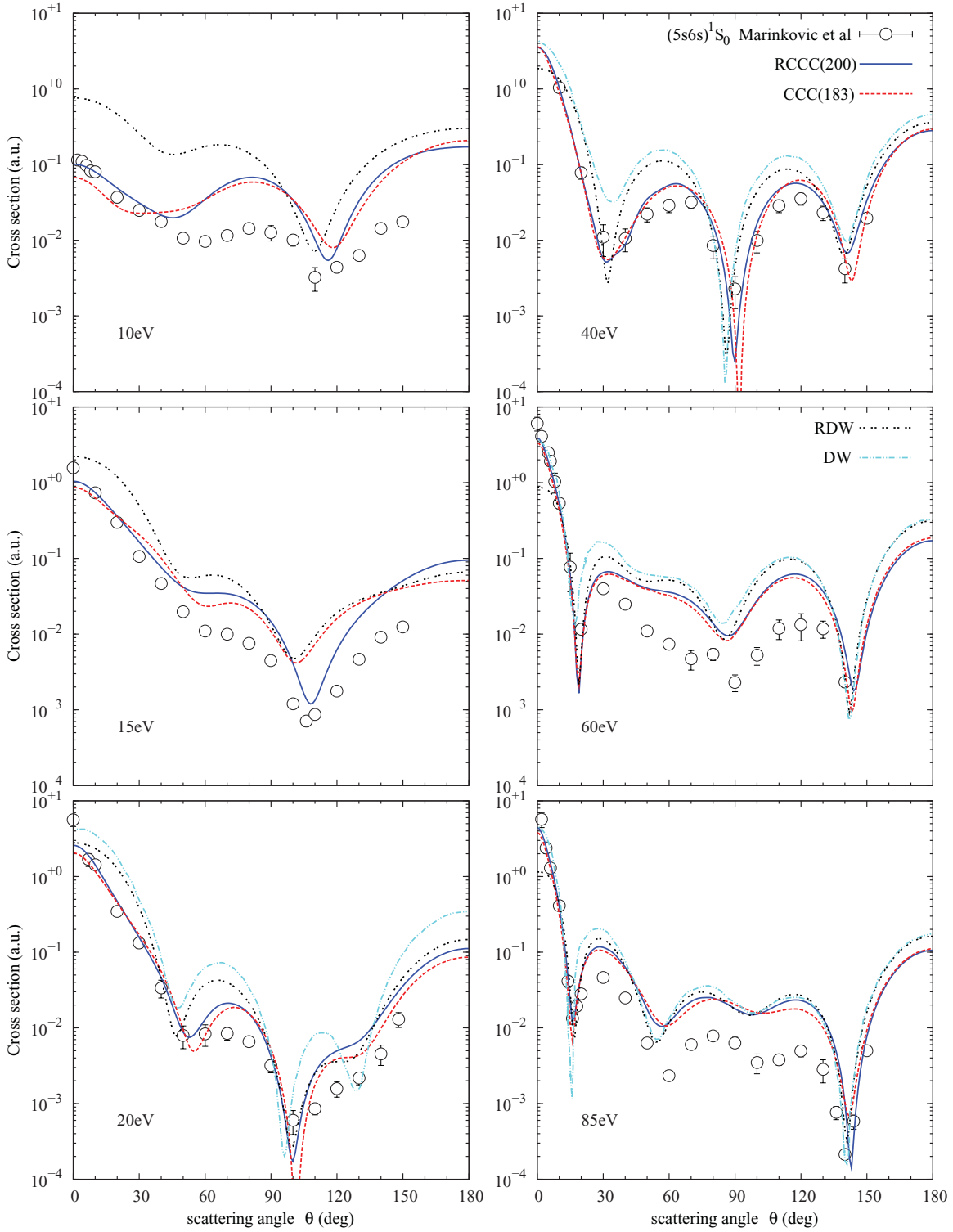

FIG. 8. (Color online) DCS for the excitation of the $(5s6s)\,^1S_0$ state of cadmium at incident electron energies of 10, 15, 20, 40, 60, and 85 eV. Theory and experiment as in Fig. 1.

reason we chose scattering angles of 10° for normalization is related to the observation that it is the lowest angle for which the experimental and theoretical GOSs have similar analytical behavior. At 10, 15, 20, and 85 eV the analytic behavior of the experimental GOS is in relatively poor agreement with the RCCC results at forward scattering angles less than 10°. This shows up in the GOS plots where the experimental results continue to rise as the angle decreases instead of turning over as the theoretical curves do at lower energies. On the other hand, at 40 and 60 eV there is excellent agreement between experiment and RCCC GOS results at all angles. Generally, all the theories and the experimental measurements show a

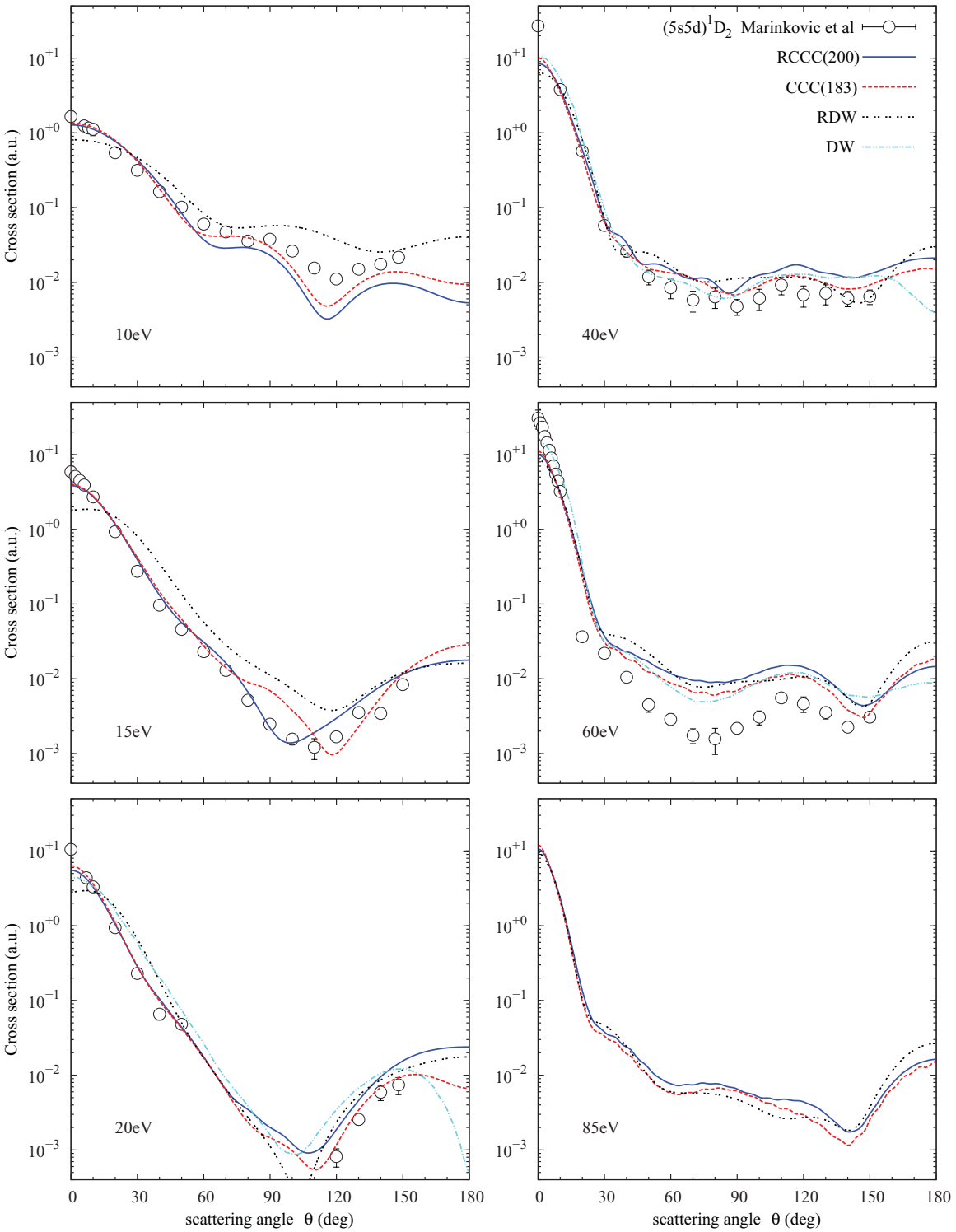

FIG. 9. (Color online) DCS for the excitation of the $(5s5d)\,^1D_2$ state of cadmium at incident electron energies of 10, 15, 20, 40, 60, and 85 eV. Theory and experiment as in Fig. 1.

similar shape for the DCS though there are differences in magnitude.

We also note the curve labeled "Born" in Figs. 1 and 2 indicates the high-energy limit and as $q \to 0$ converges to the optical oscillator strength limit. The close-coupling results are substantially below the Born limit at incident electron energies below 20 eV, which indicates that interchannel coupling is important and first-order methods might be inaccurate at low and intermediate energies.

In Figs. 3–14, DCSs are presented for elastic scattering and excitation of various states at several incident electron energies. Similar to the resonance transition, the relative

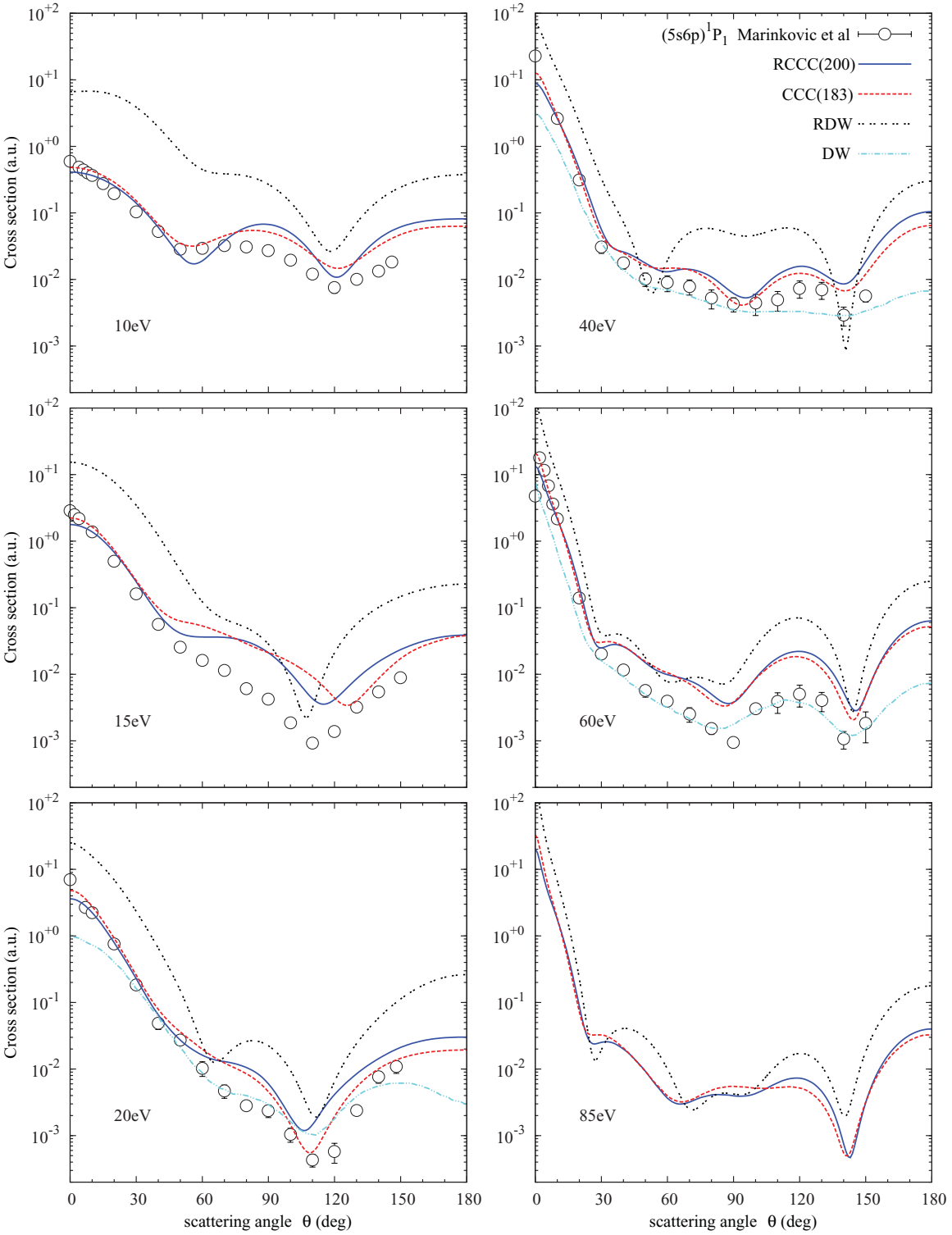

FIG. 10. (Color online) DCS for the excitation of the $(5s6p)\,^1P_1$ state of cadmium at incident electron energies of 10, 15, 20, 40, 60, and 85 eV. Theory and experiment as in Fig. 1.

experimental results of Marinkovic *et al.* [4] were normalized to the RCCC results at 10°. In a number of cases where the experimental value at 10° was not available we normalized experiment at the next available angle or by a best visual fit. In general for most of the DCSs presented, very good agreement is found between our theoretical results and the experimental measurements. Excitation of the $(5s5p)\,^3P_1$ state, Figs. 3 and 4, is the only transition where the RCCC method is clearly superior to the semirelativistic CCC, RDW, and DW methods. The DCSs presented in Fig. 4 show the rise of the DCS at forward scattering angles that is characteristic for optically allowed transitions. This transition is affected by relativistic

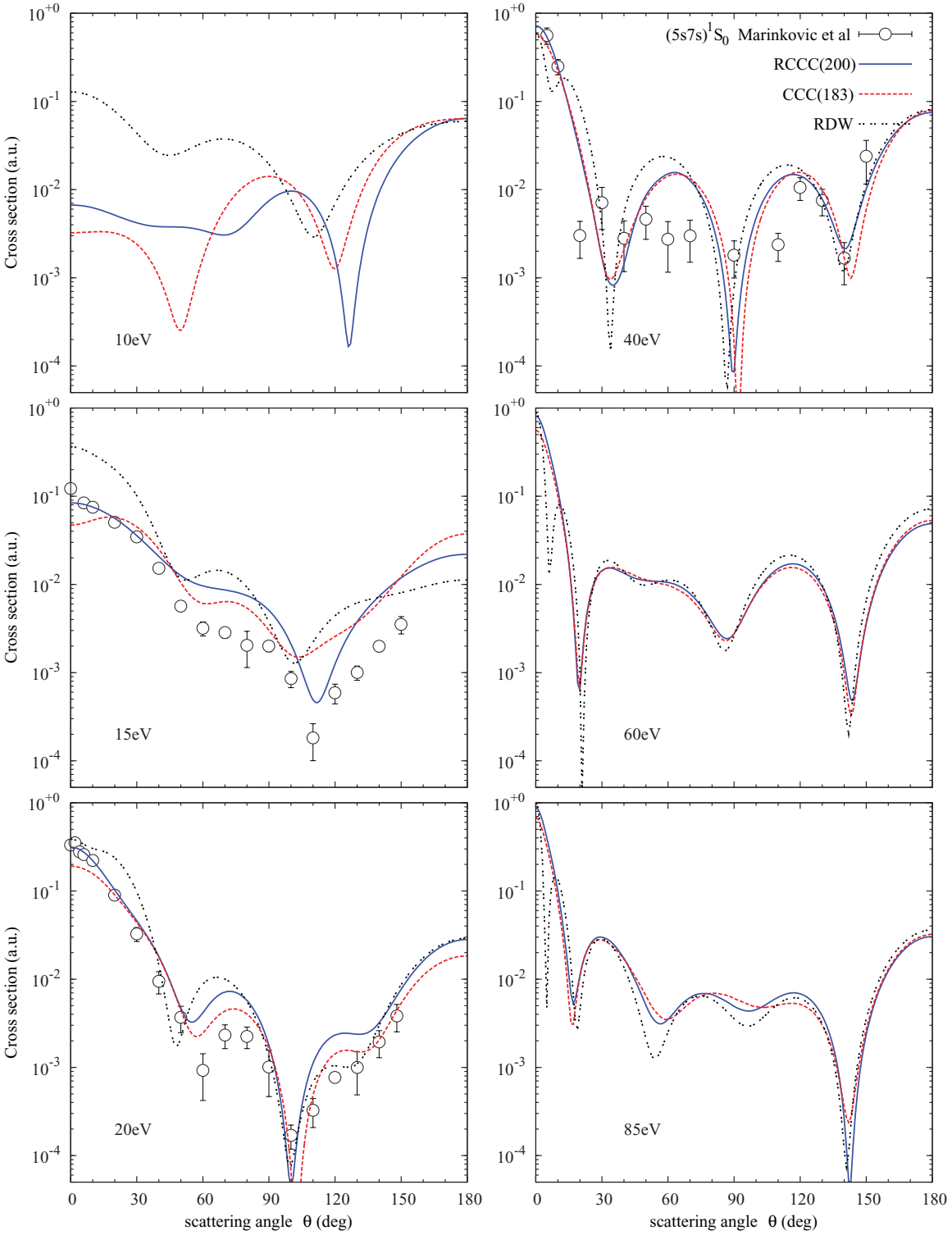

FIG. 11. (Color online) DCS for the excitation of the $(5s7s)\,^1S_0$ state of cadmium at incident electron energies of 10, 15, 20, 40, 60, and 85 eV. Theory and experiment as in Fig. 1.

effects that mix singlets and triplets; their account within the semirelativistic CCC method is apparently not adequate at incident electron energies below 40 eV. The RDW results are in generally good agreement with RCCC and CCC methods at large incident electron energies; however, energies up to 20 eV seem to be too small for such a first-order method to be valid.

The measured DCS for the $(5s5p)\,^3P_2$ state presented in Figs. 3 and 5 are in poorer agreement with the present calculations than for the $(5s5p)\,^3P_1$ state. The sharp rise in

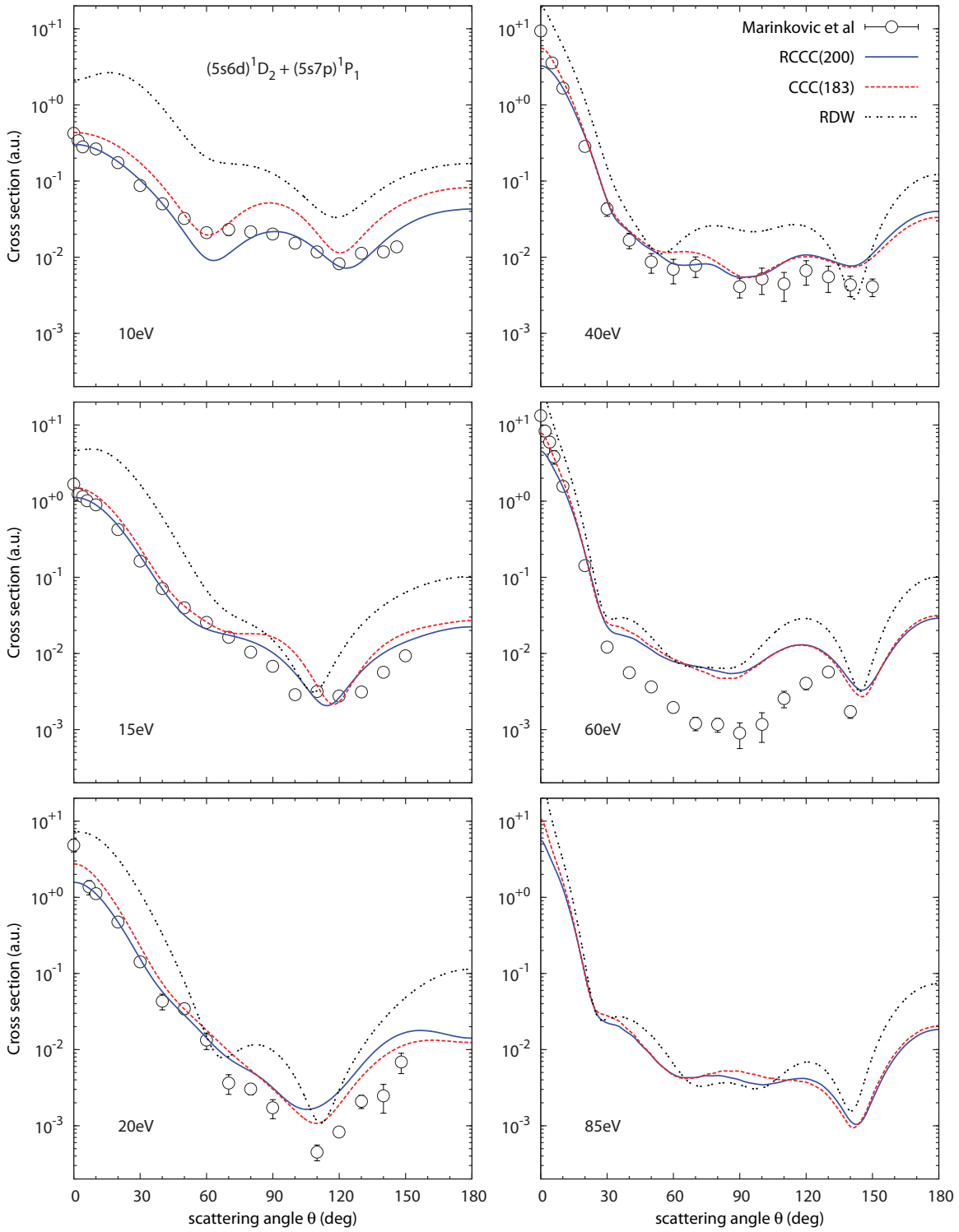

FIG. 12. (Color online) DCS for the excitation of the $(5s6d)\,^1D_2$ and $(5s7p)\,^1P_1$ states of cadmium at incident electron energies of 10, 15, 20, 40, 60, and 85 eV. Theory and experiment as in Fig. 1.

the experimental DCS at small angles for 15 and 20 eV is not supported by the theory which predicts flat or decreasing DCS, though there are large discrepancies in absolute values between close-coupling (RCCC, CCC) and first-order results (RDW, DW). At these two energies we normalized the experimental DCS at 30° which provides the best visual fit. Interestingly, the best agreement between theory and experiment is achieved at the lowest (6.4 eV) and the largest (40 eV) available energies. At 40 eV the RCCC, RDW, and DW results are in good agreement between themselves and experiment while the semirelativistic CCC DCS differs quite substantially.

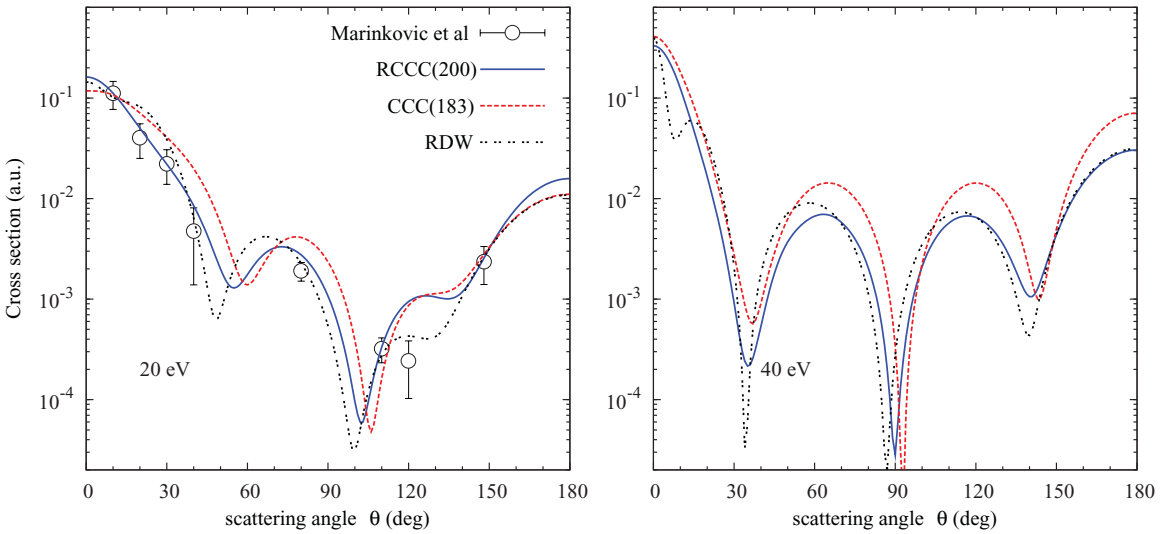

FIG. 13. (Color online) DCS for the excitation of the $(5s8s)\,{}^1S_0$ state of cadmium at incident electron energies of 20 and 40 eV. Theory and experiment as in Fig. 1.

Elastic-scattering DCSs are presented in Fig. 6. We generally observe good agreement between all theoretical results (RCCC, CCC, ROP, DW) and the experiments of Marinkovic *et al.* [4] and Nogueira *et al.* [5]. At high energies (40,

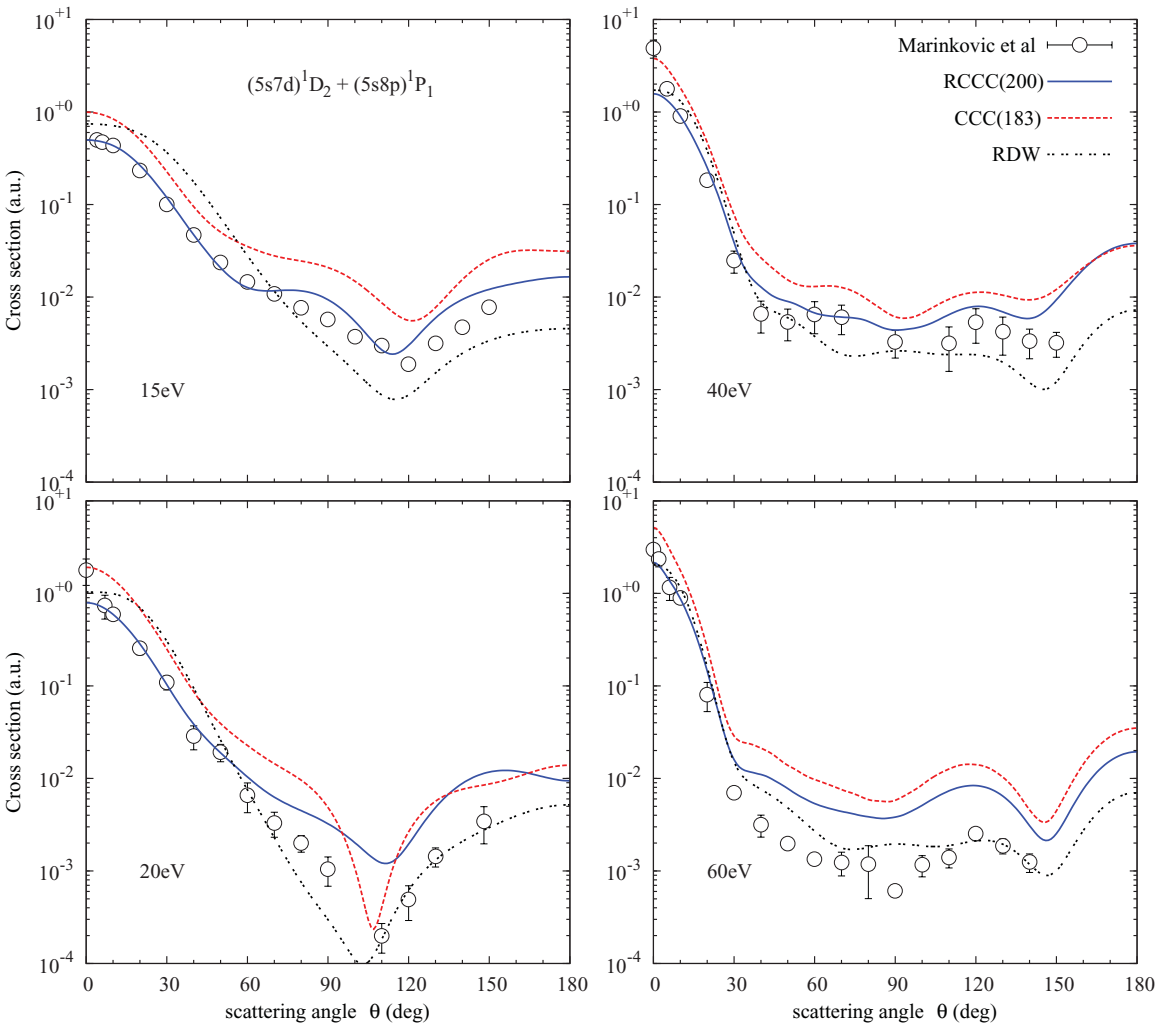

FIG. 14. (Color online) DCS for the excitation of the $(5s7d)\,{}^1D_2$ and $(5s8p)\,{}^1P_1$ states of cadmium at incident electron energies of 15, 20, 40, and 60 eV. Theory and experiment as in Fig. 1.

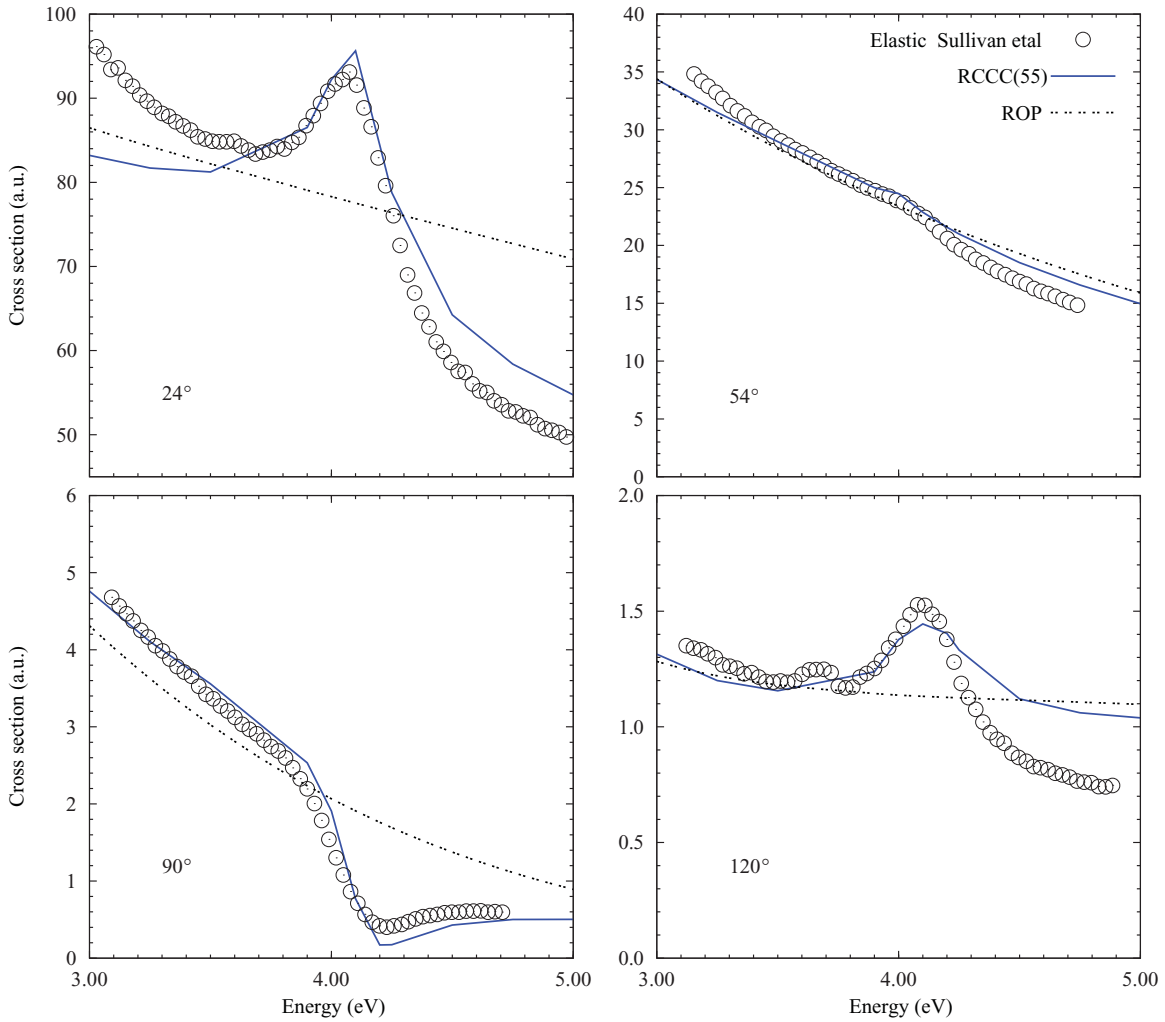

FIG. 15. (Color online) High-energy-resolution elastic DCSs at energies between 3 and 5 eV at scattering angles of 24°, 54°, 90°, and 120°. Present RCCC(55) and ROP methods are described in the text. The experimental results are due to Sullivan *et al.* [6] and have been normalized to the RCCC result for best visual fit.

60, and 85 eV) normalization of the experiment to RCCC results at 30° leads to the best agreement. Note that at these energies the RCCC and CCC calculations underestimate experiment at small scattering angles. This is consistent with the underestimation of the static dipole polarizability of Cd in the RCCC and CCC models. The ROP results are in much better agreement with experiment for those cases because the model utilizes a potential with the dipole polarizability scaled to the experimental value. There is a good agreement between ROP and DW results at 40, 60, and 85 eV for intermediate and large scattering angles. At 20 eV ROP and DW results are quite different, which is likely due to the failure of the local exchange approximation employed in DW calculations. For small scattering angles the DW results are substantially below all other theoretical results and experiment due to lack of account of intermediate state dipole contribution [10].

Agreement between the present theoretical results and experiment for the excitation of the $(5s6s)\,^3S_1$ state (see Fig. 7), is rather poor, especially at the lowest available energies of 6.4 and 10 eV where the disagreement in shape is substantial. However, for excitations of the singlet states, $(5s6s)\,^1S_0$ in Fig. 8, $(5s5d)\,^1D_2$ in Fig. 9, $(5s6p)\,^1P_1$ in Fig. 10, $(5s7s)\,^1S_0$ in Fig. 11, $(5s6d)\,^1D_2$ and $(5s7p)^1P_1$ in Fig. 12, $(5s8s)\,^1S_0$ in Fig. 13, $(5s7d)\,^1D_2$ and $(5s8p)\,^1P_1$ in Fig. 14, the present close-coupling results are in very good agreement between themselves and with experiment. The RDW and DW calculations are in good agreement with RCCC and CCC results for $(5s5d)\,^1D_2$ state excitations for energies above 20 eV, and in fair agreement for most of the remaining states.

Sullivan *et al.* [6] have found numerous resonance structures in low-energy *e*-Cd scattering. The strongest resonance feature was at 4.05 eV and was attributed to $(5s5p^2)\,^2D_{3/2,5/2}$ negative-ion states. Our calculations support this classification. This resonance is clearly seen in the high-energy-resolution experimental measurements of Sullivan *et al.* [6] taken at a number of scattering angles (see Fig. 15). We have plotted experimental DCSs against our 55-state RCCC calculation. The experimental DCS results are on a relative scale and so have been normalized to the RCCC values for the best visual fit. There is good qualitative agreement with the shape of the RCCC results and the shape of the experiment. The ROP calculations are also shown in Fig. 15; they do not exhibit

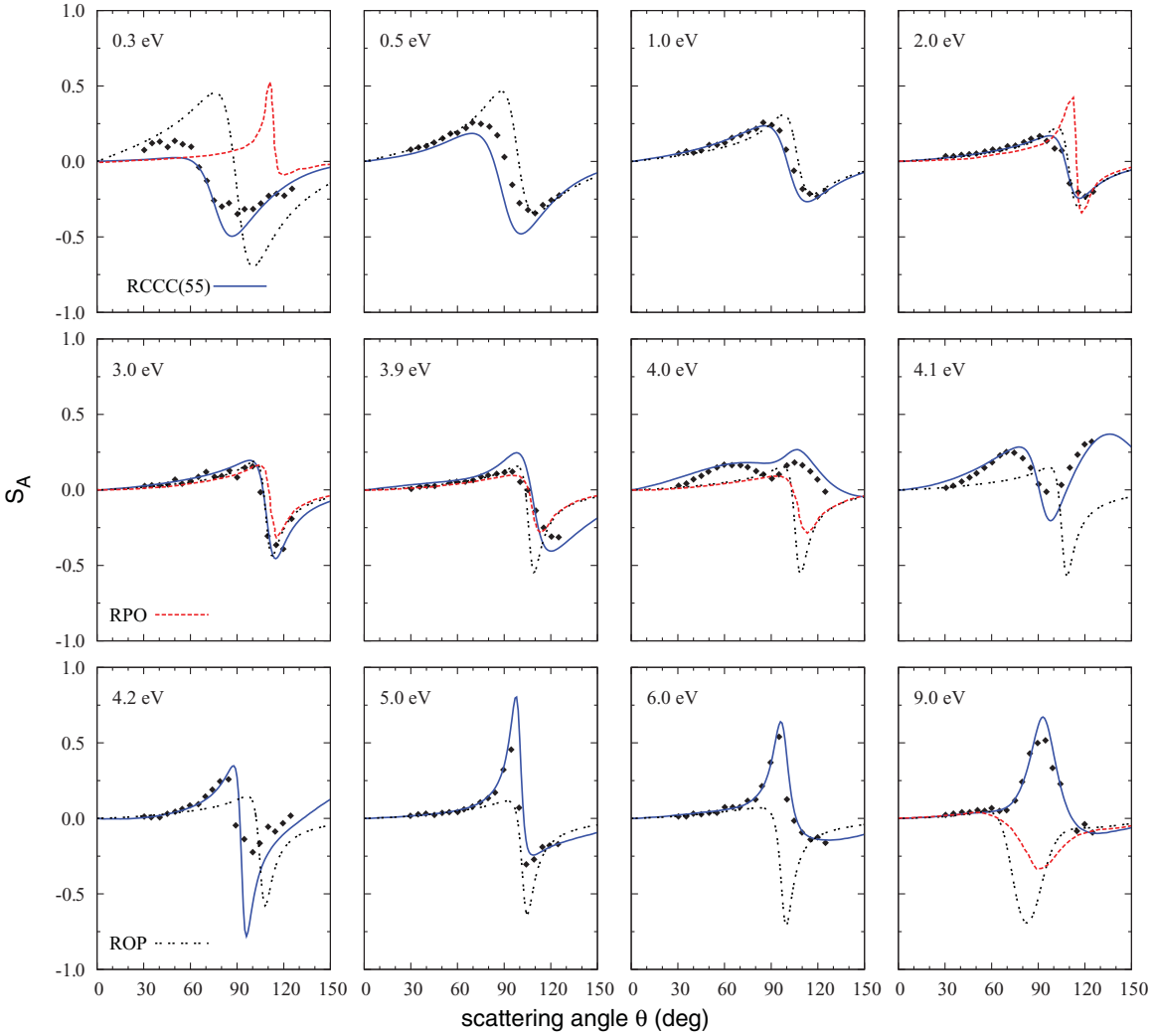

FIG. 16. (Color online) Spin-asymmetry parameter S_A at a range of energies and angles for the elastic electron scattering on cadmium. Measurements of Bartsch *et al.* [8] are presented. Present RCCC(55) and ROP calculations are described in the text. RPO results are due to Szmytkowski and Sienkiewicz [14].

any resonance behavior as expected from a single-channel method. Our RCCC(55) results show significant improvement over the five-state Breit-Pauli R-matrix calculations presented by Sullivan *et al.* [6] in the shape of the cross sections and the position of the resonance features. The most significant difference though is in the absolute values of the cross sections with our results being about an order of magnitude lower.

B. Spin-asymmetry parameter

In Fig. 16 we present the spin-asymmetry parameter (Sherman function) S_A for elastic e-Cd scattering at various incident energies. The nonrelativistic CCC theory gives identically zero for S_A due to an absence of spin-orbit coupling in the scattering formalism. The ROP results and relativistic polarized orbital (RPO) calculations of Szmytkowski and Sienkiewicz [14] often disagree with each other and differ significantly from experimental results. The RCCC results, on the other hand, are in excellent agreement with experiment across all energies. We note the RCCC method can describe the rapid variation in the shape and magnitude of S_A as the electron energy progresses through the region in the vicinity of 4 eV. This rapid variation of the Sherman function is a signature of the elastic channel coupling to the $(5s5p)\,^3P_{0,1,2}$ states (which begin to open in

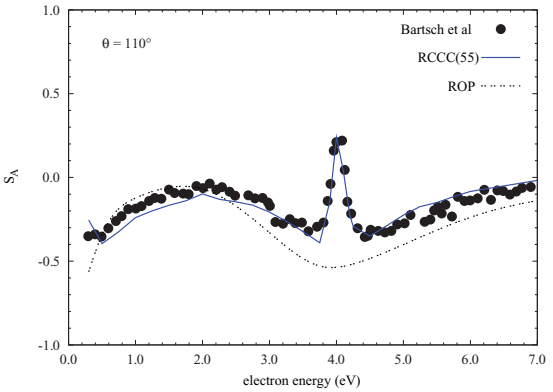

FIG. 17. (Color online) Spin-asymmetry parameter S_A as a function of energy for the elastic electron scattering on cadmium. Theory and experiment as in Fig. 16.

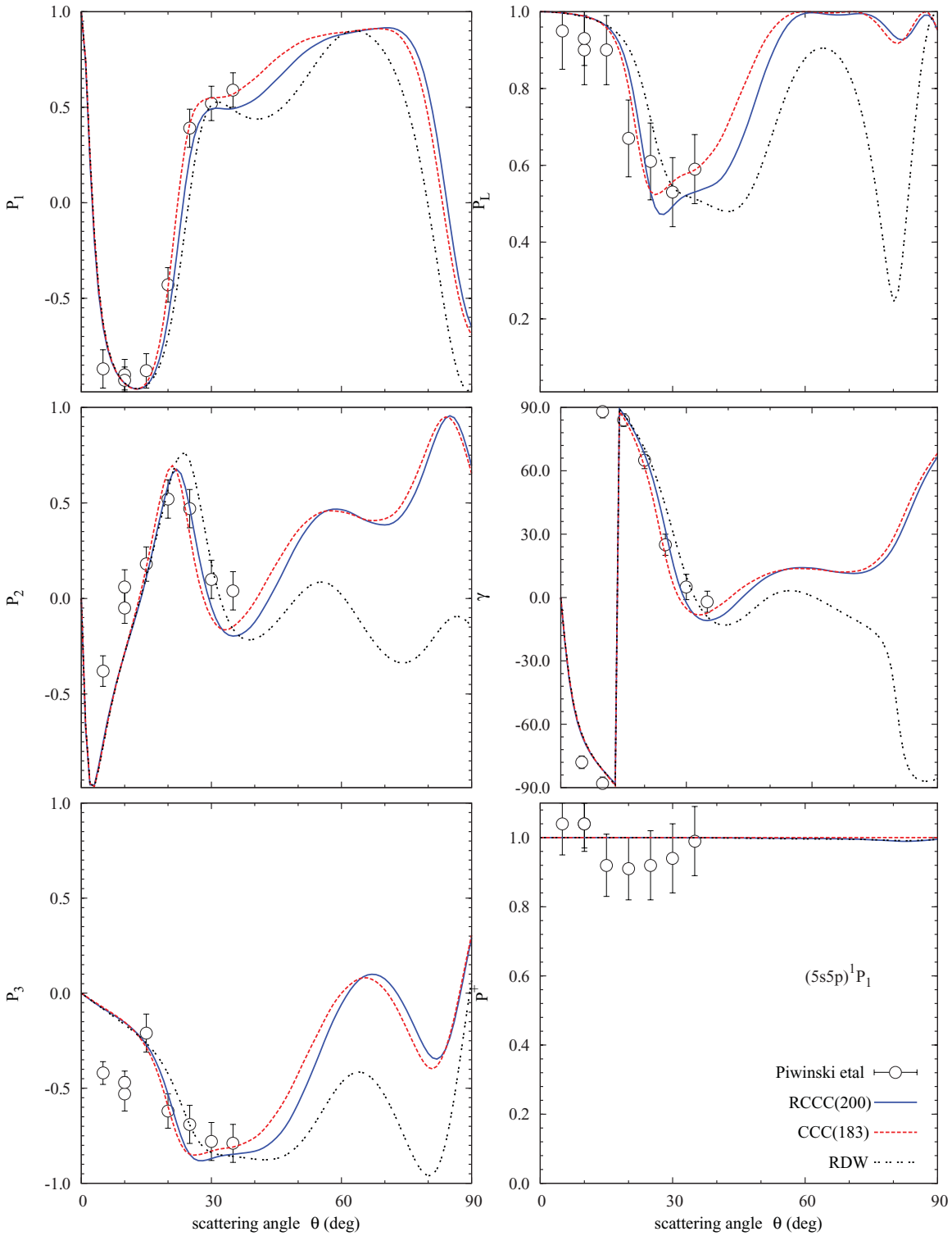

FIG. 18. (Color online) Stokes parameters (P_1, P_2, P_3) and EICPs (P_L, γ, P_+) for the excitation of the $(5s5p)\,^1P_1$ state of cadmium by 60 eV electrons. Present RCCC, CCC, and RDW calculations are described in the text. The experimental results are due to Piwinski *et al.* [7].

this energy region; see Table I) as well as the formation of $(5s5p^2)\,^2D_{3/2,5/2}$ negative-ion resonances in the same energy region. The unitarity of the close-coupling formalism accounts for the influence of excited states and resonances on the elastic channel spin asymmetry [15].

In Fig. 17 we present the results of the RCCC and ROP calculations for the spin-asymmetry parameter S_A as a function of incident projectile energy. The detector is placed at $\theta = 110^\circ$. The presence of the rapid variation in the spin-asymmetry parameter is illustrated in a conspicuous

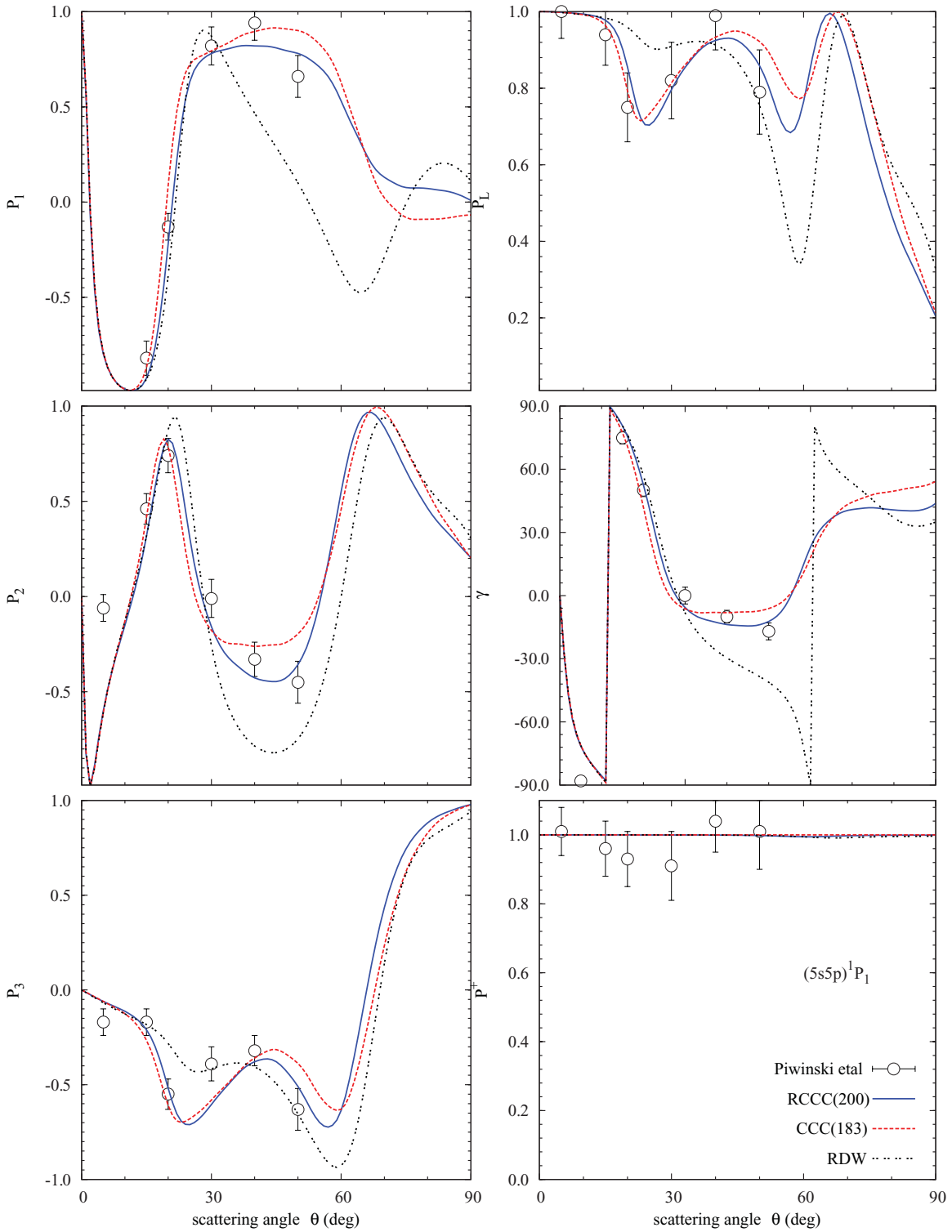

FIG. 19. (Color online) Same as in Fig. 18 but at incident electron energies of 80 eV.

manner in both the measurements and the RCCC calculations, which are in excellent agreement with each other. Once again, the unitarity of the RCCC method accounts for the elastic channel coupling to the $(5s5p)\,^3P_{0,1,2}$ excited states and $(5s5p^2)\,^2D_{3/2,5/2}$ negative-ion state which produces the rapid variation in the calculated spin-asymmetry parameter in the region between 3.8 and 4.2 eV.

C. Electron-impact coherence parameters

In Figs. 18, 19, and 20 we present RCCC, CCC, and RDW Stokes parameters (P_1, P_2, P_3) and EICPs (P_L, γ, P_+) for the excitation of the $(5s5p)\,^1P_1$ state of cadmium and compare with the experimental results of Piwinski *et al.* [7]. In some cases RCCC fares marginally better than CCC and RDW theory. Interestingly, the RDW results are in better agreement with

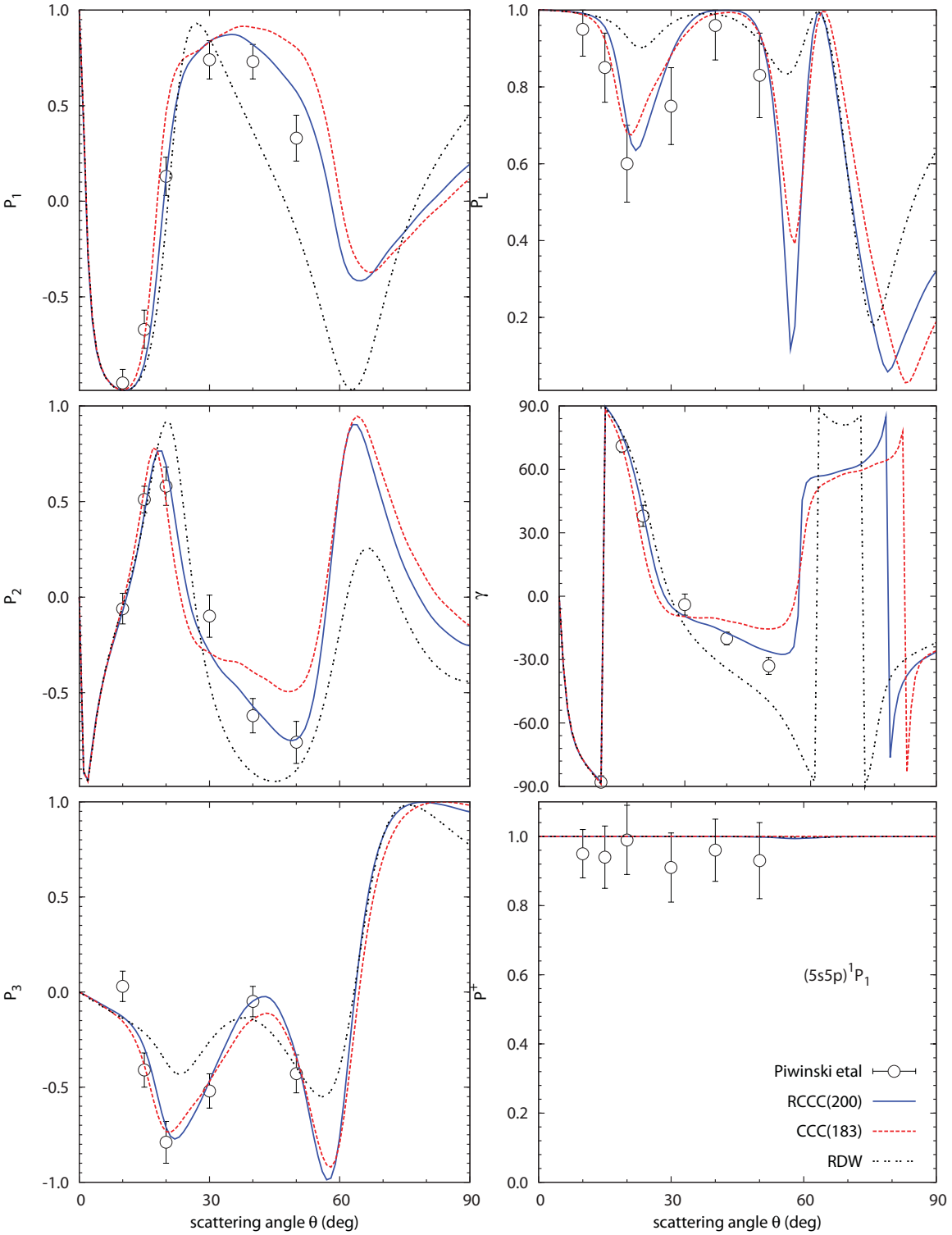

FIG. 20. (Color online) Same as in Fig. 18 but at incident electron energies of 100 eV.

experiment at the lowest available energy of 60 eV rather than at the largest energy of 100 eV. At low scattering angles there is an unresolved discrepancy between theory and experiment for the P_2 and P_3 Stokes parameters at 60 and 80 eV. At 100 eV a discrepancy exists for the low-angle P_3 Stokes parameter. Given a very good agreement between all presented theoretical methods for those cases where the disagreement with experiment seems to persist, we believe that another look at the experiment is justifiable.

IV. CONCLUSION

We have presented results of RCCC, CCC, ROP and RDW calculations for electron scattering from cadmium over a wide

range of observables in the energy range from threshold to 100 eV. There is generally satisfactory agreement between the experimental measurements and the various theories. However, we would encourage absolute measurements for the various cross sections considered here as a more stringent test of the theoretical models. Certain parameters clearly show the superiority of a relativistic model over a non- or semirelativistic one. For the Sherman function calculations, we highlight that there is a significant change in the shape, magnitude, and sign of the experimental results in the vicinity of the resonance region around 4 eV, and these changes are reproduced by the RCCC calculations but not by the CCC or ROP theories. The small-angle behavior of the $(5s5p)\,^3P_1$-state DCSs is another example where a relativistic formulation is clearly superior. For the majority of other transitions we find that an accurate account of interchannel coupling is more important than a fully relativistic treatment. We note that there is still an unresolved discrepancy between theory and experiment for the P_2 and P_3 Stokes parameters at small scattering angles.

ACKNOWLEDGMENTS

Support of the Australian Research Council and Curtin University is acknowledged. We are grateful for access to the Australian National Computational Infrastructure and its Western Australian node iVEC. RCCC calculations were performed on the EPIC supercomputer funded under the Pawsey Project. This research was partially supported by an NSERC Canada grant to A.D.S.

[1] I. Žutić, J. Fabian, and S. Das Sarma, Rev. Mod. Phys. **76**, 323 (2004).
[2] P. Kotissek, M. Bailleul, M. Sperl, A. Spitzer, D. Schuh, W. Wegscheider, C. Back, and G. Bayreuther, Nat. Phys. **3**, 872 (2007).
[3] I. Bialynicki-Birula and T. Sowiński, Phys. Rev. A **76**, 062106 (2007).
[4] B. Marinkovic, V. Pejcev, D. Filipovic, and L. Vuskovic, J. Phys. B **24**, 1817 (1991).
[5] J. C. Nogueira, W. R. Newell, and W. M. Johnston, J. Phys. B **20**, L537 (1987).
[6] J. P. Sullivan, P. D. Burrow, D. S. Newman, K. Bartschat, J. A. Michejda, R. Panajotovic, M. Moghbelalhossein, R. P. McEachran, and S. J. Buckman, New J. Phys. **5**, 159 (2003).
[7] M. Piwinski, D. Dziczek, L. Klosowski, R. Srivastava, and S. Chwirot, J. Phys. B **39**, 1945 (2006).
[8] M. Bartsch, H. Geesmann, G. F. Hanne, and J. Kessler, J. Phys. B **25**, 1511 (1992).
[9] N. Sherman, Phys. Rev. **103**, 1601 (1956).
[10] D. H. Madison, K. Bartschat, and R. Srivastava, J. Phys. B **24**, 1839 (1991).
[11] R. Srivastava, T. Zuo, R. P. McEachran, and A. D. Stauffer, J. Phys. B **25**, 1073 (1992).
[12] R. Srivastava, T. Zuo, R. P. McEachran, and A. D. Stauffer, J. Phys. B **25**, 4033 (1992).
[13] R. P. McEachran and A. D. Stauffer, J. Phys. B **25**, 1527 (1992).
[14] R. Szmytkowski and J. E. Sienkiewicz, J. Phys. B **27**, 555 (1994).
[15] C. J. Bostock, M. J. Berrington, D. V. Fursa, and I. Bray, Phys. Rev. Lett. **107**, 093202 (2011).
[16] C. J. Bostock, D. V. Fursa, and I. Bray, Phys. Rev. A **80**, 052708 (2009).
[17] D. V. Fursa and I. Bray, Phys. Rev. Lett. **100**, 113201 (2008).
[18] D. V. Fursa, C. J. Bostock, and I. Bray, Phys. Rev. A **80**, 022717 (2009).
[19] M. Maslov, M. J. Brunger, P. J. O. Teubner, O. Zatsarinny, K. Bartschat, D. Fursa, I. Bray, and R. P. McEachran, Phys. Rev. A **77**, 062711 (2008).
[20] C. J. Bostock, D. V. Fursa, and I. Bray, Phys. Rev. A **82**, 022713 (2010).
[21] C. J. Bostock, D. V. Fursa, and I. Bray, Phys. Rev. A **83**, 052710 (2011).
[22] C. J. Bostock, J. Phys. B **44**, 083001 (2011).
[23] K. G. Dyall, I. P. Grant, C. T. Johnson, F. P. Parpia, and E. P. Plummer, Comput. Phys. Commun. **55**, 425 (1989).
[24] I. P. Grant and H. M. Quiney, Phys. Rev. A **62**, 022508 (2000).
[25] D. V. Fursa and I. Bray, J. Phys. B **30**, 5895 (1997).
[26] D. V. Fursa, I. Bray, and G. Lister, J. Phys. B **36**, 4255 (2003).
[27] W. R. Johnson, D. Kolb, and K. N. Huang, At. Data Nucl. Data Tables **28**, 333 (1983).
[28] A. Ye and G. Wang, Phys. Rev. A **78**, 014502 (2008).
[29] Y. Ralchenko, A. E. Kramida, J. Reader, and NIST ASD Team, *NIST Atomic Spectra Database (Version 4.10)* (2011).
[30] J. R. Fuhr and W. L. Wiese, *CRC Handbook of Chemistry and Physics*, 86th ed. (CRC Press, Boca Raton, FL, 2005).
[31] A. Lurio and R. Novick, Phys. Rev. **134**, A608 (1964).
[32] D. Goebel and U. Hohm, Phys. Rev. A **52**, 3691 (1995).
[33] D. V. Fursa and I. Bray, Phys. Rev. A **52**, 1279 (1995).
[34] J. Migdalek and W. E. Baylis, J. Phys. B **19**, 1 (1986).
[35] P. W. Zetner, S. Trajmar, I. Kanik, S. Wang, G. Csanak, R. E. H. Clark, J. Abdallah Jr., D. V. Fursa, and I. Bray, J. Phys. B **32**, 5123 (1999).
[36] K. Hasenburg, D. H. Madison, K. Bartschat, and K. Blum, J. Phys. B **19**, 1803 (1986).
[37] S. Chen, R. P. McEachran, and A. D. Stauffer, J. Phys. B **41**, 025201 (2008).
[38] M. Vos, R. P. McEachran, G. Cooper, and A. P. Hitchcock, Phys. Rev. A **83**, 022707 (2011).
[39] I. P. Grant, B. J. McKenzie, P. H. Norrington, D. F. Mayers, and N. C. Pyper, Comput. Phys. Commun. **21**, 207 (1980).